Inorg. Chem. **2005**, *44*, 5161–5175

Tuning Tetranuclear Manganese–Oxo Core Electronic Properties: Adamantane-Shaped Complexes Synthesized by Ligand Exchange

Christopher E. Dubé,[†,‡] Sumitra Mukhopadhyay,[†,§] Peter J. Bonitatebus, Jr.,[†,∥] Richard J. Staples,[⊥] and William H. Armstrong*[,†]

Department of Chemistry, Eugene F. Merkert Chemistry Center, Boston College, Chestnut Hill, Massachusetts 02467-3860, and Department of Chemistry and Chemical Biology, Harvard University, Cambridge, Massachusetts 02138

Received February 3, 2005

A series of adamantane-shaped $[Mn_4O_6]^{4+}$ aggregates has been prepared. Ligand substitution reactions of $[Mn_4O_6(bpea)_4](ClO_4)_4$ (**1**) with tridentate amine and iminodicarboxylate ligands in acetonitrile affords derivative clusters $[Mn_4O_6(tacn)_4](ClO_4)_4$ (**4**), $[Mn_4O_6(bpea)_2(dien)_2](ClO_4)_4$ (**5**), $[Mn_4O_6(Medien)_4](ClO_4)_4$ (**6**), $[Mn_4O_6(tach)_4](ClO_4)_4$ (**7**), $[Mn_4O_6(bpea)_2(me\text{-}ida)_2]$ (**8**), $[Mn_4O_6(bpea)_2(bz\text{-}ida)_2]$ (**9**), $[Mn_4O_6(bpea)_2(^t bu\text{-}ida)_2]$ (**10**), and $[Mn_4O_6(bpea)_2(^c pent\text{-}ida)_2]$ (**11**) generally on the order of 10 min with retention of core nuclearity and oxidation state. Of these complexes, only **4** had been synthesized previously. Characterization of two members of this series by X-ray crystallography reveals that compound **7** crystallizes as $[Mn_4O_6(tach)_4](ClO_4)_4 \cdot 3CH_3CN \cdot 4.5H_2O$ in the cubic space group $Fm\bar{3}m$ and compound **11** crystallizes as $[Mn_4O_6(bpea)_2(^c pent\text{-}ida)_2] \cdot 7MeOH$ in the monoclinic space group $C2/c$. The unique substitution chemistry of **1** with iminodicarboxylate ligands afforded asymmetrically ligated complexes **8**–**11**, the mixed ligand nature of which is most likely unachievable using self-assembly synthetic methods. A special feature of the iminodicarboxylate ligand complexes **8**–**11** is the substantial site differentiation of the oxo bridges of the $[Mn_4O_6]^{4+}$ cores. While there are four site-differentiated oxo bridges in **8**, the solution structural symmetry of $\mathbf{8}H^+$ reveals essentially a single protonation isomer, in contrast to the observation of two protonation isomers for $\mathbf{1}H^+$, one for each of the site-differentiated oxo bridges in **1**. Magnetic susceptibility measurements on **4**, **7**, **8**, and **9** indicate that each complex is overall ferromagnetically coupled, and variable-field magnetization data for **7** and **9** are consistent with an $S = 6$ ground state. Electrochemical analysis demonstrates that ligand substitution of bpea affords accessibility to the $Mn^{V}(Mn^{IV})_3$ oxidation state.

Introduction

The molecular oxygen essential to life on earth is produced by the light-driven catalytic oxidation of water by photosystem II (PSII). Simultaneously, the oxygen-evolving complex (OEC) of PSII supplies the reducing equivalents employed by PSI in providing most of life's chemical energy. The OEC stores oxidizing equivalents in a series of steps (S-states) known as the Kok cycle, culminating in the oxidation of water and the release of O_2. Key components of the OEC include a compact, magnetically coupled tetranuclear manganese−oxo complex, Ca^{2+} and Cl^- cofactors, and a redox-active tyrosine residue, Y_z.[1−6] Despite the host of biophysical methods used to examine the OEC, an accurate model for the active site manganese aggregate has not been forthcoming. X-ray crystal structures of PSII from cyanobacteria *Thermosynechococcus elongatus*[7] and *Thermosynechococcus vulcanus*[8] reveal density attributed to the manganese cluster for the first time. Pertinent electron density

* E-mail: armstwi@bc.edu.
† Department of Chemistry, Eugene F. Merkert Chemistry Center, Boston College, Chestnut Hill, Massachusetts 02467-3860.
‡ Present address: Evergreen Solar, Marlborough, Massachusetts 01752.
§ Present address: Department of Chemistry, Massachusetts Institute of Technology, Cambridge, Massachusetts 02139.
∥ Present address: Emerging Technologies Laboratory PSCT, GE Global Research Center CEB 138, Niskayuna, NY 12309.
⊥ Department of Chemistry and Chemical Biology, Harvard University, Cambridge, Massachusetts 02138.

(1) Mukhopadhyay, S.; Mandal, S. K.; Bhaduri, S.; Armstrong, W. H. *Chem. Rev.* **2004**, *104*, 3981−4026.
(2) Barber, J. *Q. Rev. Biophys.* **2003**, *36*, 71−89.
(3) Carrell, T. G.; Tyryshkin, A. M.; Dismukes, G. C. *J. Biol. Inorg. Chem.* **2002**, *7*, 2−22.
(4) Siegbahn, P. E. M. *Inorg. Chem.* **2000**, *39*, 2923−2935.
(5) Penner-Hahn, J. E., *Structural Characterization of the Mn Site in the Photosynthetic Oxygen-Evolving Complex*; Springer-Verlag: Berlin, 1998; Vol. 90, pp 1−36.
(6) Yachandra, V. K.; Sauer, K.; Klein, M. P. *Chem. Rev.* **1996**, *96*, 2927−2950.

10.1021/ic050183w CCC: $30.25
Published on Web 06/17/2005

data are consistent with three manganese ions arranged in an approximate isosceles triangle, with a fourth manganese ion located near the center of the triangle. Electron density data for *T. vulcanus* also supports the assignment of the C-terminal carboxyl group of D1 Ala344 as a ligand to the manganese aggregate, as well as a number of other D1 aspartate, glutamate, and histidine residues as additional possible ligands. More recently the structure of PSII from *T. elongatus* identified the electron density attributed to four manganese ions and a fifth metal ion, which was modeled as Ca^{2+}.[9] Similar to the previous study with *T. elongatus*, several D1 aspartate, glutamate, and histidine residues were proposed as possible ligands for the manganese cluster, as well as a CP43 aspartate, although in the present study the C-terminal carboxyl group of Ala344 is not coordinated to the metal cluster. It should be noted, however, that uncertainties associated with these X-ray structures, as well as possible irradiation effects,[10] make it difficult to assign atom connectivity within the manganese aggregate as well as between the metal cluster and associated peptide residues. Mn···Mn distances in these structures are approximately 3 Å. These data are similar to those obtained with extended X-ray absorption fine structure (EXAFS) studies of the S_2 state, which indicate at least two 2.7 Å Mn···Mn vectors, as well as a longer 3.3 Å Mn···Mn (or Mn···Ca) vector.[6,11−14] Although precise details of the ligand environment remain an area of active investigation, it is believed that the Mn complex is coordinated predominantly by oxide and carboxylates (i.e. aspartate and glutamate) and one or two imidazoles.[8,9,15−17]

Insight into the structure and mechanism of action of the OEC has been achieved through synthesis, characterization, and reactivity studies of high-valent tetranuclear manganese−oxo aggregates, such as the adamantane-shaped $[Mn_4(\mu\text{-}O)_6]^{4+}$,[18−22] $[Mn_4(\mu\text{-}O)_6]^{3+}$,[21−24] $[Mn_4(\mu\text{-}O)_5(OH)]^{5+}$,[20,21] and $[Mn_4(\mu\text{-}O)_4(OH)_2]^{6+}$;[25] open chain $[Mn_4(\mu\text{-}O)_6]^{4+}$[26−28] and $[Mn_4(\mu\text{-}O)_6]^{3+}$ cores;[29] the cubane-like $[Mn_4(\mu_3\text{-}O)_3(\mu_3\text{-}X)]^{4+}$,[30−33] $[Mn_4(\mu_3\text{-}O)_4]^{6+}$,[34, 35] and $[Mn_4(\mu_3\text{-}O)_4]^{7+}$;[36] the butterfly-shaped $[Mn_4(\mu_3\text{-}O)_2(\mu\text{-}OAc)_7]^{+}$;[37−40] a stacked dimer-of-dimers $[Mn_2(\mu\text{-}O)_2(\mu\text{-}OR)]_2^{4+}$,[41−43] an open dimer-of-dimers $[Mn_4(\mu\text{-}O)_5]^{6+}$;[44] and an open species $[Mn_4(\mu\text{-}O)_5]^{6+}$.[45]

Consideration of PSII biophysical studies as well as of the coordination chemistry of manganese has led to a number of proposals for the mechanism of photosynthetic O_2 evolution. Of particular note here are EXAFS studies comparing the S_2 and S_3 states. EXAFS data suggest that advancement from S_2 to S_3 is accompanied by structural changes in the PSII Mn_4 complex, although these studies have led to very different conclusions. In one study, these changes have been interpreted in terms of formation of an additional μ-oxo bridge between Mn atoms.[46,47] In another

(7) Zouni, A.; Witt, H.-T.; Kern, J.; Fromme, P.; Krauss, N.; Saenger, W.; Orth, P. *Nature* **2001**, *409*, 739−743.
(8) Kamiya, N.; Shen, J.-R. *Proc. Natl. Acad. Sci. U.S.A.* **2003**, *100*, 98−103.
(9) Ferreira, K. N.; Iverson, T. M.; Maghlaoui, K.; Barber, J.; Iwata, S. *Science* **2004**, *303*, 1831−1838.
(10) Dau, H.; Liebisch, P.; Haumann, M. *Phys. Chem. Chem. Phys.* **2004**, *6*, 4781−4792.
(11) Kirby, J. A.; Robertson, A. S.; Smith, J. P.; Thompson, A. C.; Cooper, S. R.; Klein, M. P. *J. Am. Chem. Soc.* **1981**, *103*, 5529−5537.
(12) Penner-Hahn, J. E.; Fronko, R. M.; Pecoraro, V. L.; Yocum, C. F.; Betts, S. D.; Bowlby, N. R. *J. Am. Chem. Soc.* **1990**, *112*, 2549−2557.
(13) MacLachlan, D. J.; Hallahan, B. J.; Ruffle, S. V.; Nugent, J. H. A.; Evans, M. C. W.; Strange, R. W.; Hasnain, S. S. *Biochem. J.* **1992**, *285*, 569−576.
(14) DeRose, V. J.; Mukerji, I.; Latimer, M. J.; Yachandra, V. K.; Sauer, K.; Klein, M. P. *J. Am. Chem. Soc.* **1994**, *116*, 5239−5249.
(15) Debus, R. J. *Biochim. Biophys. Acta* **2001**, *1503*, 164−186.
(16) Diner, B. A. *Biochim. Biophys. Acta* **2001**, *1503*, 147−163.
(17) Debus, R. J.; Aznar, C.; Campbell, K. A.; Gregor, W.; Diner, B. A.; Britt, R. D. *Biochemistry* **2003**, *42*, 10600−10608.
(18) Wieghardt, K.; Bossek, U.; Gebert, W. *Angew. Chem., Int. Ed. Engl.* **1983**, *22*, 328−329.
(19) Wieghardt, K.; Bossek, U.; Nuber, B.; Weiss, J.; Bonvoisin, J.; Corbella, M.; Vitols, S. E.; Girerd, J. J. *J. Am. Chem. Soc.* **1988**, *110*, 7398−7411.
(20) Hagen, K. S.; Westmoreland, T. D.; Scott, M. J.; Armstrong, W. H. *J. Am. Chem. Soc.* **1989**, *111*, 1907−1909.
(21) Dubé, C. E.; Wright, D. W.; Pal, S.; Bonitatebus, P. J., Jr.; Armstrong, W. H. *J. Am. Chem. Soc.* **1998**, *120*, 3704−3716.
(22) Visser, H.; Dubé, C. E.; Armstrong, W. H.; Sauer, K.; Yachandra, V. K. *J. Am. Chem. Soc.* **2002**, *124*, 11008−11017.
(23) Dubé, C. E.; Sessoli, R.; Hendrich, M. P.; Gatteschi, D.; Armstrong, W. H. *J. Am. Chem. Soc.* **1999**, *121*, 3537−3538.
(24) Dubé, C. E.; Wright, D. W.; Armstrong, W. H. *Angew. Chem., Int. Ed.* **2000**, *39*, 2169−2172.
(25) Dubé, C. E.; Wright, D. W.; Armstrong, W. H. *J. Am. Chem. Soc.* **1996**, *118*, 10910−10911.
(26) Dunand-Sauthier, M.-N. C.; Deronzier, A.; Piron, A.; Pradon, X.; Menage, S. *J. Am. Chem. Soc.* **1998**, *120*, 5373−5380.
(27) Philouze, C.; Blondin, G.; Menage, S.; Auger, N.; Girerd, J.; Vigner, D.; Lance, M.; Nierlich, M. *Angew. Chem., Int. Ed. Engl.* **1992**, *31*, 1629−1631.
(28) Philouze, C.; Blondin, G.; Girerd, J.; Guilhem, J. *J. Am. Chem. Soc.* **1994**, *116*, 8557−8565.
(29) Blondin, G.; Davydov, R.; Philouze, C.; Charlot, M.-F.; Styring, S.; Åkermark, B.; Girerd, J.-J.; Boussac, A. *J. Chem. Soc., Dalton Trans.* **1997**, 4069−4074.
(30) Hendrickson, D. N.; Christou, G.; Schmitt, E. A.; Libby, E.; Baskin, J. S.; Wang, S.; Tsai, H.; Vincent, J. B.; Boyd, P. D. W.; Haffman, J. C.; Folting, K.; Li, Q.; Streib, W. E. *J. Am. Chem. Soc.* **1992**, *114*, 2455−2471.
(31) Wemple, M. W.; Tsai, H.-L.; Folting, K.; Hendrickson, D. N.; Christou, G. *Inorg. Chem.* **1993**, *32*, 2025−2031.
(32) Wemple, M. W.; Adams, D. M.; Folting, K.; Hendrickson, D. N.; Christou, G. *J. Am. Chem. Soc.* **1995**, *117*, 7275−7276.
(33) Aromi, G.; Wemple, M. W.; Aubin, S. J.; Folting, K.; Hendrickson, D. N.; Christou, G. *J. Am. Chem. Soc.* **1998**, *123*, 5850−5851.
(34) Ruettinger, W. F.; Campana, C.; Dismukes, G. C. *J. Am. Chem. Soc.* **1997**, *119*, 6670−6671.
(35) Ruettinger, W.; Yagi, M.; Wolf, K.; Bernasek, S.; Dismukes, G. C. *J. Am. Chem. Soc.* **2000**, *122*, 10353−10357.
(36) Ruettinger, W. F.; Ho, D. M.; Dismukes, G. C. *Inorg. Chem.* **1999**, *38*, 1036−1037.
(37) Vincent, J. B.; Christmas, C.; Chang, H. R.; Li, Q.; Boyd, P. D. W.; Huffman, J. C.; Hendrickson, D. N.; Christou, G. *J. Am. Chem. Soc.* **1989**, *111*, 2086−2097.
(38) Libby, E.; McCusker, J. K.; Schmitt, E., A.; Folting, K.; Hendrickson, D. N.; Christou, G. *Inorg. Chem.* **1991**, *30*, 3486-3495.
(39) Grillo, V. A.; Knapp, M. J.; Bollinger, J. C.; Hendrickson, D. N.; Christou, G. *Angew. Chem., Int. Ed. Engl.* **1996**, *35*, 1818−1820.
(40) Sanudo, E. C.; Grillo, V. A.; Knapp, M. J.; Bollinger, J. C.; Huffman, J. C.; Hendrickson, D. N.; Christou, G. *Inorg. Chem.* **2002**, *41*, 2441−2450.
(41) Chan, M. K.; Armstrong, W. H. *J. Am. Chem. Soc.* **1991**, *113*, 5055−5057.
(42) Kirk, M. L.; Chan, M. K.; Armstrong, W. H.; Solomon, E. I. *J. Am. Chem. Soc.* **1992**, *114*, 10432−10440.
(43) Mukhopadhyay, S.; Mok, H. J.; Staples, R. J.; Armstrong, W. H. *J. Am. Chem. Soc.* **2004**, *126*, 9202−9204.
(44) Chen, H.; Faller, J. W.; Crabtree, R. H.; Brudvig, G. W. *J. Am. Chem. Soc.* **2004**, *126*, 7345−7349.
(45) Mukhopadhyay, S.; Staples, R. J.; Armstrong, W. H. *J. Chem. Soc., Chem. Commun.* **2002**, 864−865.
(46) Dau, H.; Iuzzolino, L.; Dittmer, J. *Biochim. Biophys. Acta* **2001**, *1503*, 24−39.

study EXAFS data were interpreted in terms of an increase in the PSII Mn_4 metal−metal distance, which was attributed to lengthening of the di μ-oxo bridges between Mn ions.[48] Among the proposed mechanisms for water oxidation, several account for S_2 to S_3 (or S_3 to S_0) advancement in terms of a significant core rearrangement, such as Mn−oxo rearrangement from a cubane to an adamantane core[49,50] and rearrangement of a butterfly to a partial cubane core.[35,51,52] Although EXAFS analysis of the active site of PSII excludes highly symmetric adamantane- or cubane-shaped Mn−oxo cores as accurate structural models of the S_0 to S_2 states, we conjecture that structural rearrangement of the Mn_4 OEC is an explanation for changes in the metal−metal distance proposed for advancement from S_2 to S_3 and S_3 to S_0. A core rearrangement demonstrated by us involves a shape shift from a dimer-of-dimers to an adamantane core.[43] Previously, we demonstrated that a dimer-of-dimers complex $[Mn_4O_4(tphpn)_2](CF_3SO_3)_4$ (**2**) (Htphpn = *N*,*N*′,*N*′-tetra(2-pyridylmethyl)-2-hydroxypropane-1,3-diamine) is a good spectral model of the PSII S_1 state of the oxygen-evolving complex.[41,42] Further investigation of the reactivity of **2** reveals that it undergoes dramatic structural changes concurrent with one-electron oxidation or reduction.[43,53] In particular, oxidation of **2** from oxidation state $(Mn^{III})_2(Mn^{IV})_2$ to $(Mn^{III})(Mn^{IV})_3$ results in a structural rearrangement to an adamantane-like core complex, $[Mn_4O_4(tphpn)_2](CF_3SO_3)_2(ClO_4)_3$ (**3**). We have also shown that **2** undergoes isomerization in solution without a redox change, as demonstrated by UV−vis and ^{1}H NMR spectroscopies.

The dimer-of-dimers and adamantane-shaped Mn−oxo cores exhibit additional reactivity relevant to water oxidation, such as protonation, reversible electron-transfer and proton-coupled electron transfer.[21,25,41,53] Both electron- and proton-transfer chemistry are critical components of the Kok cycle[54] as well as various proposed mechanisms for water oxidation that emphasize the deprotonation of H_2O to form terminal or bridging OH^- or O^{2-} ligands at the active site. Recent proposals suggest the participation of a Mn(IV)[55,56] or Mn(V)[57−61] terminal Mn═O group in the course of O−O bond formation.[62] Furthermore, $(Mn^{IV})_3Mn^V$ is one of the proposed oxidation state assignments for the OEC S_4 state.[57,63,64] For these reasons, an understanding of the factors that influence the protonation and redox behavior of tetranuclear manganese−oxo clusters is essential in order to activate a core toward substrate oxidation.

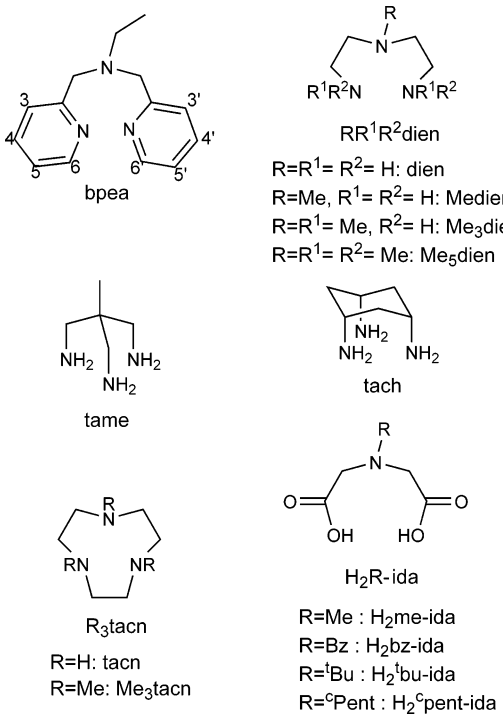

Figure 1. Ligands discussed in this paper.

In an ongoing effort to understand the formation and physical properties of manganese−oxo clusters, we have extended our reactivity studies of Mn−oxo cores coordinated with *N*,*N*-bis(2-pyridylmethyl)ethylamine (bpea) (Figure 1).[21,65−68] Previously, we showed that the adamantane-like complex $[Mn_4O_6(bpea)_4](ClO_4)_4$ (**1**) exhibits reversible protonation, electron-transfer, and proton-coupled electron transfer.[21] Here we report the ligand substitution reactivity of **1**. Whereas self-assembly of aggregates frequently relies on assembling the thermodynamic product(s), the ligand-sub-

(47) Haumann, M.; Grabolle, M.; Neisius, T.; Dau, H. *FEBS Lett.* **2002**, *512*, 116−120.
(48) Liang, W.; Roelofs, T. A.; Cinco, R. M.; Rompel, A.; Latimer, M. J.; Yu, W. O.; Sauer, K.; Klein, M. P.; Yachandra, V. K. *J. Am. Chem. Soc.* **2000**, *122*, 3399−3412.
(49) Brudvig, G. W.; Crabtree, R. H. *Proc. Natl. Acad. Sci. U.S.A.* **1986**, *83*, 4586−4588.
(50) Brudvig, G. W.; De Paula, J. C., Progress in Photosynthesis Research. In *Progress in Photosynthesis Research*; Biggins, J., Ed.; Martinus Nijhoff: The Hague, 1987; Vol. 1, pp 490−498.
(51) Christou, G.; Vincent, J. B. *Biochim. Biophys. Acta* **1987**, *895*, 259−274.
(52) Christou, G.; Vincent, J. B. *Structural types in oxide-bridged manganese chemistry: toward a model of the photosynthetic water oxidation center*; Washington, 1988; Vol. 1988; p 238−255.
(53) Armstrong, W. H.; Mukhopadhyay, S.; Mok, H. J. *J. Inorg. Biochem.* **2001**, *86*, 130.
(54) Kok, B.; Forbrush, B.; McGloin, M. *Photochem. Photobiol.* **1970**, *11*, 457−475.
(55) Hoganson, C. W.; Babcock, G. T. *Science* **1997**, *277*, 1953−1955.
(56) Tommos, C.; Babcock, G. T. *Acc. Chem. Res.* **1998**, *31*, 18−25.
(57) Vrettos, J. S.; Brudvig, G. W. *Philos. Trans. R. Soc. London B* **2002**, *357*, 1395−1405.
(58) Vrettos, J. S.; Limburg, J.; Brudvig, G. W. *Biochim. Biophys. Acta* **2001**, *1503*, 229−245.
(59) Limburg, J.; Vrettos, J. S.; Liable-Sands, L. M.; Rheingold, A. L.; Crabtree, R. H.; Brudvig, G. W. *Science* **1999**, *283*, 1524−1527.
(60) Law, N. A.; Caudle, M. T.; Pecoraro, V. L. *Adv. Inorg. Chem.* **1998**, *46*, 305−440.
(61) Barber, J.; Ferreira, K.; Maghlaoui, K.; Iwata, S. *Phys. Chem. Chem. Phys.* **2004**, *6*, 4737−4742.
(62) Although formation of a Mn(V)═O species in the S_3 state is not supported by comparison of the XANES spectrum of a model Mn(V)═O compound with spectra of the S_2 and S_3 states of the OEC (*J. Am. Chem. Soc.* **2004**, *126*, 8070−8071), formation of a Mn(V)═O species in the S_4 state cannot be ruled out.
(63) Dau, H.; Liebisch, P.; Haumann, M. *Anal. Bioanal. Chem.* **2003**, *376*, 562−583.
(64) Iuzzolino, L.; Dittmer, J.; Doerner, W.; Meyer-Klaucke, W.; Dau, H. *Biochemistry* **1998**, *37*, 17112−17119.
(65) Pal, S.; Chan, M.; Armstrong, W. H. *J. Am. Chem. Soc.* **1992**, *114*, 6398−6406.
(66) Pal, S.; Olmstead, M. M.; Armstrong, W. H. *Inorg. Chem.* **1995**, *34*, 4708−4715.
(67) Mandal, S. K.; Armstrong, W. H. *Inorg. Chim. Acta* **1995**, *229*, 261−270.
(68) Mok, H. J.; Davis, J. A.; Pal, S.; Mandal, S. K.; Armstrong, W. H. *Inorg. Chim. Acta* **1997**, *263*, 385−394.

Table 1. Designation of Compounds

$[Mn_4O_6(bpea)_4](ClO_4)_4$	**1**
$[Mn_4O_6(tacn)_4](ClO_4)_4$	**4**
$[Mn_4O_6(bpea)_2(dien)_2](ClO_4)_4$	**5**
$[Mn_4O_6(Medien)_4](ClO_4)_4$	**6**
$[Mn_4O_6(tach)_4](ClO_4)_4$	**7**
$[Mn_4O_6(bpea)_2(me\text{-}ida)_2]$	**8**
$[Mn_4O_6(bpea)_2(bz\text{-}ida)_2]$	**9**
$[Mn_4O_6(bpea)_2(^t bu\text{-}ida)_2]$	**10**
$[Mn_4O_6(bpea)_2(^c pent\text{-}ida)_2]$	**11**

stituted product will be determined by kinetic as well as thermodynamic factors. Furthermore, we sought to use ligands such as iminodicarboxylates (Figure 1) that more closely approximate the coordination environment of PSII yet are too reactive under the highly oxidizing conditions typically utilized in self-assembly of high-valent manganese−oxo complexes. Also, we wished to explore the possibility of generating asymmetrically ligated clusters. Finally, it was hoped that substitution of the bpea ligand on the adamantane-shaped core with ligands possessing different characteristics would alter the reactivity of the $[Mn_4O_6]^{4+}$ core, promote core rearrangement, and provide access to a Mn(V) species. Herein we report the synthesis and characterization of a series of adamantane-shaped $[Mn_4O_6]^{4+}$ complexes, as designated in Table 1. In this paper, a comparison of spectroscopic and redox properties is presented as well as X-ray structure determinations for two members of the series. Furthermore, the pK_a value is established for two members of the series.

Experimental Section

Abbreviations. The following abbreviations are used throughout this paper: Fc/Fc^+, ferrocene/ferricenium ion $Fe^{II}(cp)_2/Fe^{III}(cp)_2^+$, where cp = cyclopentadienyl; TBAP, tetrabutylammonium perchlorate; bpea, *N*,*N*-bis(2-pyridylmethyl)ethylamine; bpta, *N*,*N*-bis-(2-pyridylmethyl)-*tert*-butylamine; bispicen, *N*,*N*′-bis(2-methylpyridyl)-1,2-ethanediamine; tmpa, tris(2-methylpyridyl)amine; tren, 2,2′,2″-triaminotriethylamine; tacn, 1,4,7-triazacyclononane; Me_3-tacn, 1,4,7-trimethyl-1,4,7-triazacyclononane; tame, 1,1,1-tris(aminomethyl)ethane; tach, *cis*,*cis*-1,3,5-triaminocyclohexane; dien, diethylenetriamine; Medien, *N*′-methyldiethylenetriamine; Me_3dien, *N*,*N*′,*N*″-trimethyldiethylenetriamine; Me_5dien, *N*,*N*,*N*′, *N*″,*N*″-pentamethyldiethylenetriamine; me-ida, *N*-methyliminodiacetate; bz-ida, *N*-benzyliminodiacetate; ^{t}bu-ida, *N*-*tert*-butyliminodiacetate; ^{c}pent-ida, *N*-cyclopentyliminodiacetate

Materials. Acetonitrile used for synthesis was distilled from CaH_2. Acetonitrile used for electrochemical and UV−vis experiments was distilled from CaH_2 and then stored over 3 Å molecular sieves for at least 1 week prior to use. Propylene carbonate was dried over 4 Å molecular sieves for at least one week and vacuum distilled just prior to use. Deuterated acetonitrile (Cambridge Isotope Laboratories, Inc.) was dried in flame-dried glassware over activated 3 Å molecular sieves. Deuterated chloroform, methanol, and water (Cambridge Isotope Laboratories, Inc.) were used as received. Tacn, Me_3tacn, H_2me-ida, and H_2bz-ida were purchased from Aldrich and used as received. Dien, Medien, Me_3dien, and Me_5dien were purchased from Aldrich and distilled under vacuum prior to use. A mixture of *cis*,*cis*- and *cis*,*trans*-1,3,5-triaminocyclohexane was purchased from Ambinter. All other reagents were purchased and used as received. Electrochemical grade TBAP (Fluka) and $AgClO_4$ (Aldrich) were used as received. Paratone-N oil was obtained from Exxon. All chemicals used in this work were of reagent grade.

Physical Methods. Electronic spectra were collected at 298 K using a Cary 1E UV−vis spectrophotometer. ^{1}H NMR data were collected at 298 K on a Varian Unity 300 MHz NMR spectrometer with a 100 kHz sweep width. All ^{1}H NMR spectra were background corrected using a first-order correction function. Peak widths at full-width half-maximum (fwhm) are in hertz. Values for chemical shifts (ppm) are the observed shifts referenced to the appropriate residual protic solvent peak ($CHCl_3$, 7.24 ppm; CHD_2CN, 1.94 ppm; CD_3OH, 4.78 ppm, CHD_2OD, 3.30 ppm; HOD, 4.68 ppm). IR spectra were recorded using a Nicolet 5DX FT-IR spectrometer using either a KBr disk or a solution cell containing an acetonitrile solution. Solid-state magnetic susceptibility measurements were performed on a Quantum Design SQUID magnetometer at either the Massachusetts Institute of Technology or Tufts University in the temperature range 2−300 K at a constant applied magnetic field of 0.5 T. Measurements at Tufts University were performed on powdered samples pressed into the small half of a gelatin capsule which was then sealed with the larger half of the capsule followed by Mylar tape. All data were corrected for the susceptibility of the empty sample container and Mylar tape, including its field dependence. Measurements at the Massachusetts Institute of Technology were performed on powdered samples pressed between cotton plugs inside a straw. All data were corrected for the susceptibility of the empty container, including its field dependence. Isothermal magnetization data were collected at 2, 5, and 10 K from 0.1 to 5.5 T. Solution magnetic susceptibility characteristics were determined by the NMR method[69−71] at 298 K. Molar paramagnetic susceptibilities were obtained by using diamagnetic corrections ($\chi_d = -586 \times 10^{-6}$, -586×10^{-6}, -561×10^{-6}, and -648×10^{-6} cgs/mol for **4**, **7**, **8** and **9**, respectively) calculated from Pascal's constants.[72] Elemental analyses were obtained from Desert Analytics, Tucson, AZ. Electrospray ionization mass spectrometry (ESI-MS) (typically 2×10^{-4} M in acetonitrile or methanol at a 3.5 kV nebulizer voltage) was performed on a Micromass Quattro mass spectrometer at the University of Illinois Mass Spectrometry Laboratory.

Electrochemistry. A BAS-100B Electrochemical Analyzer was used for electrochemical experiments. A platinum disk working electrode and a platinum wire auxiliary electrode were used to collect cyclic voltammograms in acetonitrile or propylene carbonate at a scan rate of 50 mV/s. An $Ag/AgClO_4$ electrode was used as the reference electrode. All electrochemical measurements employed 0.1 M TBAP as supporting electrolyte. Cyclic voltammetry of Fc in the appropriate solvent was determined during electrochemical analysis of compounds. The $E_{1/2}$ values of the Fc/Fc^+ couple in acetonitrile and propylene carbonate were typically 106 and 72 mV, respectively. Potentials are reported versus the Fc/Fc^+ couple.[73] All electrochemical measurements were performed under a dry and purified N_2 atmosphere. The potentials reported in this work are uncorrected for a junction contribution.

Ligand Synthesis. The ligand bpea was prepared as described elsewhere.[66−68] Synthesis of *N*-cyclopentyliminodiacetic acid and *N*-*tert*-butyliminodiacetic acid, $H_2{}^c$pent-ida and $H_2{}^t$bu-ida, respectively, followed modifications[74] of the method of Berchet[75] and are given in detail in the Supporting Information. Synthesis of tame and tach was based on modifications[76] of the method of Fleischer

(69) Evans, D. J. *J. Chem. Soc.* **1959**, 2003−2005.
(70) Dickinson, W. C. *Phys. Rev.* **1951**, *81*, 717−731.
(71) Live, D. H.; Chan, S. I. *Anal. Chem.* **1971**, *42*, 791−792.
(72) Mulay, L. N., Theory and Applications of Molecular Paramagnetism. In *Theory and Applications of Molecular Paramagnetism*; Boudreaux, E. A., Mulay, L. N., Eds.; Wiley: New York, 1976.
(73) Connelly, N. G.; Geiger, W. E. *Chem. Rev.* **1996**, *96*, 877−910.
(74) Chase, B. H.; Downes, A. M. *J. Chem. Soc.* **1953**, 3874−3877.
(75) Berchet, G. J. *Organic Syntheses*; Wiley: New York, 1943; Collect Vol. II, pp 397−399.
(76) Bollinger, J. E.; Mague, J. T.; Banks, W. A.; Kastin, A. J.; Roundhill, D. M. *Inorg. Chem.* **1995**, *34*, 2143-2152.

et al.[77] Synthesis of tach is described in Supporting Information. **Caution!** *Polyazides are potentially explosive.*[78] Alternatively, tach was purified from a mixture of *cis,cis*-and *cis,trans*-1,3,5-triaminocyclohexane following the method of Wentworth[79] and is described in Supporting Information. The free base of tame and tach used for substitution chemistry were prepared under anhydrous conditions by dissolving the trihydrochloride salts in methanol and adding a stoichiometric amount of NaOMe and stirring briefly. The resulting solid was filtered off and the solvent removed by rotary evaporation to yield a white solid. This was dissolved in acetonitrile and filtered and the solvent removed to yield the free base as a fine white powder.

The *N*-alkyl quaternary ammonium salts (n-Bu_4N^+ or Et_4N^+) of H_2R-ida ligands were prepared by stoichiometric addition of an aqueous solution of either (n-Bu_4N)OH or (Et_4N)OH to an aqueous solution of H_2R-ida, where R denotes the substituent on the imine nitrogen atom. The majority of the solvent was removed by rotary evaporation to obtain a viscous oil and the final drying was done on a vacuum line. The dried *N*-alkyl quaternary ammonium salts of H_2R-ida are hygroscopic and were recrystallized under anhydrous conditions. See Table S1 for yields, elemental analyses, and ^{1}H NMR data for these ligands.

Complex Synthesis. $[Mn_4O_6(bpea)_4](ClO_4)_4$ (1), $[Mn_4O_6(bpea)_4](CF_3SO_3)_4$, and **$[Mn_4O_6(bpea)_4]Br_4$** were prepared as described previously.[21]

$[Mn_4O_6(tacn)_4](ClO_4)_4$ (4). An acetonitrile solution (1.0 mL) of tacn (0.080 g, 0.616 mmol) was added to an acetonitrile solution (25 mL) of **1** (0.222 g, 0.137 mmol) over 10 min. The reaction mixture was allowed to stir for 1 h and then the solution was concentrated to about 1 mL by rotary evaporation. The product was precipitated by dropwise addition of the acetonitrile solution to 3 mL of vigorously stirred diethyl ether. The dark purple precipitate was collected by filtration and washed with diethyl ether and dried in vacuo to give 0.156 g (0.127 mmol, 93%) of **4** as a dark purple powder. Diffusion of chloroform into an acetonitrile solution (3 mL) of **4** (0.156 g, 0.127 mmol) at room temperature gave purple hexagonal plates of **4** (0.148 g, 0.121 mmol, 88%). See Table S2 for yields, elemental analyses and ESI-MS data, Table S3 for UV−vis, $E_{1/2}$, and IR data, and Table S4 for ^{1}H NMR data for this and other compounds in this section.

Preparation of $[Mn_4O_6(tacn)_4](CF_3SO_3)_4$ was done in an entirely analogous manner using $[Mn_4O_6(bpea)_4](CF_3SO_3)_4$. Complex $[Mn_4O_6(tacn)_4](CF_3SO_3)_4$ was crystallized from vapor diffusion of chloroform into an acetonitrile solution of it at room temperature.

$[Mn_4O_6(dien)_2(bpea)_2](ClO_4)_4$ (5). An acetonitrile solution (2.5 mL) of dien (0.040 g, 0.385 mmol) was added to an acetonitrile solution (20 mL) of **1** (0.250 g, 0.154 mmol) over 30 min with an addition funnel. The solution was allowed to stir for an additional 3 h and then the solution was concentrated to 2 mL by rotary evaporation. The product was precipitated by dropwise addition of the acetonitrile solution to 5 mL of vigorously stirred diethyl ether. The dark brown precipitate was collected by filtration and washed with diethyl ether and dried in vacuo to give 0.171 g (0.125 mmol, 81%) of **5** as a dark brown powder. Diffusion of $CHCl_3$ into an acetonitrile solution (4 mL) of **5** (0.171 g, 0.125 mmol) at room temperature gave thin dendritic black plates of **5** (0.166 g, 0.121 mmol, 79%).

$[Mn_4O_6(Medien)_4](ClO_4)_4$ (6). An acetonitrile solution (2 mL) of Medien (0.084 g, 0.704 mmol) was added to an acetonitrile solution (20 mL) of **1** (0.254 g, 0.156 mmol) over 10 min. The reaction was allowed to stir for an additional 30 min and then the solution was concentrated to 1 mL by rotary evaporation. The product was precipitated by dropwise addition of the acetonitrile solution to 3 mL of vigorously stirred diethyl ether. The dark brown precipitate was collected by filtration and washed with diethyl ether and dried in vacuo to give 0.130 g (0.110 mmol, 70%) of **6** as a dark brown powder. Diffusion of $CHCl_3$ into an acetonitrile solution (4 mL) of **6** (0.130 g, 0.110 mmol) at room temperature gave microcrystalline **6** (0.116 g, 0.098 mmol, 62%).

$[Mn_4O_6(tach)_4](ClO_4)_4$ (7). A methanol solution (0.5 mL) of tach (0.100 g, 0.773 mmol) was added to an acetonitrile solution (20 mL) of **1** (0.167 g, 0.103 mmol) over 10 min. The reaction was allowed to stir for 6 h and then the solution was concentrated to dryness using rotary evaporation. The dark purple precipitate was triturated with EtOH to remove excess tach and dried in vacuo to give 0.126 g (0.102 mmol, 99%) of **7** as a dark purple powder. Diffusion of diethyl ether into an acetonitrile solution (3 mL) of **7** (0.126 g, 0.102 mmol) at −20 °C gave purple hexagonal plates of **7** (0.108 g, 0.088 mmol, 85%).

Ligand substitution reactions with hygroscopic $[Et_4N]_2$[R-ida] and $[n$-$Bu_4N]_2$[R-ida] ligands were performed under prepurified argon with standard glovebox techniques.

$[Mn_4O_6(bpea)_2(me\text{-}ida)_2]$ (8). An acetonitrile solution (5 mL) of $[n$-$Bu_4N]_2$[me-ida] (0.214 g, 0.340 mmol) was added dropwise to a stirred acetonitrile solution (20 mL) of **1** (0.250 g, 0.154 mmol) over 15 min. The reaction was allowed to stir for an additional 15 min, after which time a light green precipitate was allowed to settle, leaving a faint red solution. The crude product was filtered under ambient conditions, washed with acetonitrile, and dried under vacuum to give 0.114 g (70%) of **8**. Vapor diffusion of acetone into an aqueous solution (3 mL) of **8** (0.114 g, 0.107 mmol) yielded fine green needles of **8** (0.0627 g, 0.059 mmol, 55%) after 3 days at room temperature.

$[Mn_4O_6(bpea)_2(^c pent\text{-}ida)_2]$ (11). An acetonitrile solution (5 mL) of $[Et_4N]_2[^c$pent-ida] (0.225 g, 0.489 mmol) was added dropwise to a stirred acetonitrile solution (15 mL) of **1** (0.318 g, 0.196 mmol) over 15 min. The reaction was allowed to stir for an additional 15 min, after which time a light green precipitate was allowed to settle, leaving a red-brown solution. The crude product was filtered under ambient conditions, washed with acetonitrile, and dried under vacuum to give 0.135 g (0.116 mmol, 59%) of **11**. The crude product was dissolved in 3 mL of MeOH and filtered. Diffusion of Et_2O into a MeOH solution (3 mL) of **11** (0.135 g, 0.116 mmol) at −20 °C gave thin rectangular plates (0.123 g, 0.106 mmol, 54%).

Complexes **9** and **10** were synthesized and crystallized according to the procedure for **11** and are described in the Supporting Information.

^{1}H NMR Titration. Protonation of 8 and 11. In a typical titration, a solution of **8** in D_2O (0.4 mL, 9.0 mM) was prepared and transferred to an NMR tube. Protonation of **8** was accomplished by addition of aliquots of $HClO_4$ (1.0 μL, 1.0 M in CD_3CN) with a gastight syringe through the septum seal of the NMR tube. Generation of **8**H(ClO_4) was considered complete when additional aliquots of $HClO_4$ gave no further change in the ^{1}H NMR spectrum. A ^{1}H-NMR-monitored titration of **11** was carried out in an entirely analogous fashion in MeOD or D_2O.

Spectrophotometric Titration. Protonation of 8 and 11. Titration of aqueous solutions of **8** and **11** was monitored spectrophotometrically and with a pH electrode. In a typical titration, the pH and absorbance spectrum of **8** (2 mL of a 4.31×10^{-4} M

(77) Fleischer, E. B.; Gebala, A. E.; Levey, A.; Tasker, P. A. *J. Org. Chem.* **1971**, *36*, 3042−3044.
(78) Spear, R. J.; Dagley, I. J., Organic Energetic Compounds. In *Organic Energetic Compounds*; Marinkas, P. L., Ed.; Nova Science Publishers: New York, 1994; pp 135−142.
(79) Wentworth, R. A. D. *Inorg. Chem.* **1968**, *7*, 1030−1032.

Table 2. Crystallographic Data for $[Mn_4O_6(tach)_4](ClO_4)_4 \cdot 3CH_3CN \cdot 4.5H_2O$ and $[Mn_4O_6(bpea)_2(^c\text{pent-ida})_2] \cdot 7MeOH$

	7·$3CH_3CN$·$4.5H_2O$	**11**·7MeOH
empirical formula	$C_{30}H_{78}Cl_4Mn_4N_{15}O_{26.5}$	$C_{53}H_{88}Mn_4N_8O_{21}$
formula weight, g/mol	1434.49	1393.05
crystal system	cubic	monoclinic
space group	$Fm\bar{3}m$	$C2/c$
a, Å	23.934(6)	10.543(2)
b, Å	23.934(6)	25.198(4)
c, Å	23.934(6)	24.295(4)
α, deg	90	90.
β, deg	90	90.28(2)
γ, deg	90	90.
volume, Å^3	13711(6)	6454.1(2)
Z	8	4
ρ(calc), g/cm^3	1.390	1.434
θ range, deg	1.47−26.39	1.82−28.19
reflections collected	22104	8775
independent reflections	765 [R(int) = 0.1499]	6424 [R(int) = 0.0303]
data/restraints/parameters	765/1/51	6264/1/368
goodness-of-fit of F^2	1.053	1.088
final R indices [$I > 2\sigma(I)$]	R1 = 0.0691, wR2 = 0.2116	R1 = 0.0634, wR2 = 0.1216

aqueous stock solution) was measured following addition of an acid such as perchloric acid ($pK_a = -1.7$, the pK_a of H_3O^+), triflic acid (CF_3SO_3H, $pK_a = -1.7$), or trifluoracetic acid ($pK_a = 0.5$).[80] Acid was added until there was no further change in the absorbance spectrum. The data were fit to the following expression, derived for the reaction $B + H^+ \leftrightarrows HB^+$

$$A_\lambda = C_o\left(\frac{(\epsilon_{HB}^{\lambda})10^{-pH} + (\epsilon_{B}^{\lambda})10^{-pK_a}}{10^{-pH} + 10^{-pK_a}}\right) \quad (1)$$

where A_λ is the absorbance at a selected wavelength, C_o is the initial concentration of the complex, and ϵ_B^λ and ϵ_{HB}^λ are the extinction coefficients of the complex and its protonated form, respectively, at the selected wavelength. Spectrophotometric titrations of **8** and **11** were monitored at 515 nm and nonlinear least-squares fitting of eq 1 to the experimental data used 1795 and 2422 for ϵ_B^λ and ϵ_{HB}^λ, respectively, for **8** and 1798 and 2361 for ϵ_B^λ and ϵ_{HB}^λ, respectively, for **11**.

X-ray Crystallography. Compound **7** crystallizes as $[Mn_4O_6(tach)_4](ClO_4)_4 \cdot 3CH_3CN \cdot 4.5H_2O$ in the cubic space group $Fm\bar{3}m$ with eight molecules in the unit cell and compound **11** crystallizes as $[Mn_4O_6(bpea)_2(^c\text{pent-ida})_2] \cdot 7MeOH$ in the monoclinic space group $C2/c$ with four molecules in the unit cell. Relevant crystal data are summarized in Table 2.

Single crystals of **7** suitable for structure determination were obtained by diffusion of diethyl ether into an acetonitrile solution of **7** at −20 °C. Single crystals of **11** suitable for structure determination were obtained by diffusion of diethyl ether into a methanol solution of **11** at −20 °C. Crystals of each were taken from the mother liquor, coated with Paratone-N oil, mounted on a glass fiber with Apiezon-T grease, and immediately transferred to the dinitrogen cold stream. Data for **7** were collected using a Bruker diffractometer equipped with a SMART-APEX CCD (charge-coupled device) detector and data for **11** were collected using a Bruker diffractometer equipped with a SMART CCD detector. The instruments used Mo Kα radiation ($\lambda = 0.71073$ Å) and included a LT-3 low-temperature apparatus operating at 193 K. Data were measured using omega scans of 0.3° per frame for 30 s, such that a hemisphere was collected. A total of 1271 frames were collected with a maximum resolution of 0.75 Å. The first 50 frames were recollected at the end of data collection to monitor for crystal decay. Crystals used for the diffraction studies showed no decomposition during data collection.

Scheme 1. Ligand Substitution Reactions of **1** in Acetonitrile

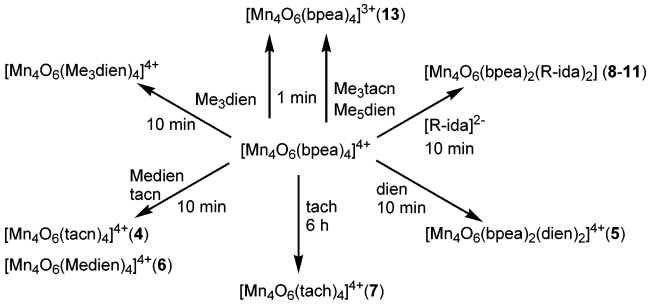

Cell parameters were retrieved using SMART[81] software and refined using SAINT[82] on all observed reflections. Data reduction was performed using the SAINT software, which corrects for Lp and decay. Absorption corrections were performed with the SADABS Program,[83] supplied by George Sheldrick. The structures were solved by direct methods using SHELXS-97[84] and refined by least-squares methods on F^2 in SHELXL-97,[85] incorporated in SHELXTL-PC V 5.10.[86] All non-hydrogen atoms were refined with anisotropic thermal parameters. Hydrogen atom positions were calculated by geometrical methods and refined using a riding model. All drawings presented here are made using 30% probability thermal ellipsoids.

Results and Discussion

Synthesis. Ligand substitution reactions of **1** are outlined in Scheme 1. Complex **1** was synthesized by comproportionation of Mn(II) and Mn(VII) starting materials in the presence of the bpea ligand.[21] We speculate that a similar synthetic approach with the primary amine and iminodicarboxylate ligands used here would have resulted in ligand oxidation in the course of self-assembly. While ligand oxidation during self-assembly can be a useful synthetic tool in the formation of new complexes, we pursued ligand substitution reactions of **1** as an initial approach.

It was anticipated that ligand substitution reactions of this core would be slow. This is because the Mn^{IV} d^3 ions , like the substitutionally inert Cr^{III},[87−89] enjoy a considerable ligand field stabilization energy (LFSE) and that ligand substitution by a dissociative (D) or interchange dissociative (I_d) mech-

(80) March, J. *Advanced Organic Chemistry*, 3rd ed.; Wiley-Interscience: New York, 1985.

(81) *SMART V 5.050 (NT) Software for the CCD Detector System*; Bruker Analytical X-ray Instruments, Inc.: Madison, WI, 1998.
(82) *SAINT V 5.01 (NT) Software for the CCD Detector System*; Bruker Analytical X-ray Instruments, Inc.: Madison, WI, 1998.
(83) Blessing, R. H. SADABS. Program for absorption corrections using Siemens CCD based on the method of Robert Blessing. *Acta Crystallogr.* **1995**, *A51*, 33−38.
(84) Sheldrick, G. M. *SHELXS-97, Program for the Solution of Crystal Structure*; University of Göttingen, Germany, 1997.
(85) Sheldrick, G. M. *SHELXL-97, Program for the Refinement of Crystal Structure*; University of Göttingen, Germany, 1997.
(86) *SHELXTL 5.10 (PC Version), Program library for Structure Solution and Molecualr Graphics*; Bruker Analytical X-ray Systems: Madison, WI, 1998.
(87) Swaddle, T. W. *Adv. Inorg. Bioinorg. Mech.* **1983**, *2*, 95−138.
(88) Swaddle, T. W. *Coord. Chem. Rev.* **1974**, *14*, 217−268.
(89) There are a number of Cr(III) complexes that are substitutionally labile (stopped-flow regime). See, for example: Beswick, C. L.; Shalders, R. D.; Swaddle, T. W. *Inorg. Chem.* **1996**, *35*, 991−994 and references therein.

anism through a trigonal bipyramidal transition state would involve a significant loss of LFSE.[90] It is unlikely that ligand substitution would proceed by an associative (A) or interchange associative (I_a) mechanism, through a 7-coordinate transition state, due to the bulky nature of the tridentate ligands. In addition, the tridentate ligands of **1** impart additional stability against ligand substitution due to the chelate effect. Also, it was unclear whether ligand substitution reactions with **1** would proceed with retention of the $[Mn_4O_6]^{4+}$ core structure or whether substitution would promote core rearrangement, aggregation, or fragmentation. Our investigations have shown that reaction of **1** with a variety of tridentate amine and iminodicarboxylate ligands in acetonitrile at room temperature produces derivative clusters **4**−**11** generally on the order of 10 min with retention of core nuclearity and oxidation state, as monitored by UV−vis and ^{1}H NMR spectroscopy. Of these complexes, only **4** had been synthesized previously.[18,20,91] Although it was not attempted, it is possible that self-assembly of several of the amine complexes, such as **6** and **7**, would have been achieved by air oxidation of a basic solution of Mn(II) and the respective ligands, analogous to the synthesis of **4**,[18,20] $[Mn_4O_5(OH)(tame)_4](CF_3SO_3)_5$,[20] $[Mn_2O_2(cyclam)_2](ClO_4)_3$,[92] and $[Mn_2O_2(tren)_2](CF_3SO_3)_3$.[93]

Reaction of **1** with the amine ligands in acetonitrile resulted in either ligand substitution, one-electron reduction of **1** to form $[Mn_4O_6(bpea)_4](ClO_4)_3$ (**13**),[21,23,24] or both. For example, reaction of **1** in acetonitrile (5×10^{-4} M) with 4.2 equiv of tacn typically produced the ligand substitution product **4** in about 10 min. On occasion, however, nonstoichiometric one-electron reduction of **1** occurred during ligand substitution reactions, requiring considerably longer times (about 2.5 h for completion, at about 86% yield) to form **4**. ^{1}H NMR confirmed the observation of rapid, yet partial, initial core reduction to **13** and the formation of tacnH$^+$, followed by slower ligand substitution over a few hours. On the other hand, reaction of **1** with the tertiary amine Me_3tacn produced only **13** and Me_3tacnH$^+$ in quantitative yield, as noted previously.[21] Reactions of **1** with the primary amines tame and tach exhibited much slower substitution kinetics. ^{1}H NMR spectra of the reaction of **1** (1.2×10^{-2} M) with the primary amine tame (up to 15 equiv) over times on the order of 24 h suggest partial substitution; thus, this reaction was not pursued further. On the other hand, reaction of **1** (5.15×10^{-3} M) with 8 equiv of the more rigid amine tach, which is conformationally predisposed for facial coordination, proceeds cleanly to the tach analogue **7** for times on the order of 6 h. Reaction of **1** with 3−8 equiv of dien resulted in isolation of the mixed ligand product $[Mn_4O_6(bpea)_2(dien)_2](ClO_4)_4$ (**5**), the structure of which has been crystallographically established and confirmed by mass spectrometry. Reaction of **1** with Medien resulted in isolation of the fully substituted product $[Mn_4O_6(Medien)_4](ClO_4)_4$ (**6**) in about 10 min, which was also confirmed by mass spectrometry. Reaction of **1** with Me_3dien gave a mixture of $[Mn_4O_6(Me_3dien)_4](ClO_4)_4$ (observed by electrospray MS $[M - ClO_4]^+ = 1195.5$; expected 1195.1) and **13** (observed by ^{1}H NMR), while reaction of **1** with Me_5dien gave only **13**.

The oxidation of tertiary amines by inorganic complexes has been explored both as a preparative tool[73,94,95] and for its enzymatic relevance.[95,96] Although often mechanistic details remain unclear, it is generally accepted that the reducing power of an amine is determined by its pK_a and not by its oxidation potential and that coordination of the amine nitrogen to the metal complex is a critical step in the electron transfer.[94,95] Most recently, oxidative transformations of amines employing transition metal catalysts, such as Ru or Co, and molecular oxygen are receiving increasing attention.[97,98] In these reports the proposed transformations involve coordination of the tertiary amine and molecular oxygen to the metal center in the initial activation steps. A recent report of the noncatalytic oxidation of tertiary amines using a $Mn^{III}Mn^{IV}$ complex proposes coordination of the amine to a metal center, although dioxygen activation is thought to occur via an amine α-radical to form an α-amino peroxide.[99]

Substitution chemistry of **1** with *N*-alkyl quaternary ammonium salts of N-substituted iminodicarboxylate ligands resulted in the neutral mixed-ligand complexes $[Mn_4O_6(bpea)_2(R\text{-ida})_2]$. There was no apparent reaction between H_2R-ida and **1** in acetonitrile for periods up to 13 h according to UV−vis and ^{1}H NMR data. *N*-Alkyl quaternary ammonium salts, rather than Na^+ or K^+ salts, were chosen for their greater solubility. Attempts to prepare a $[Mn_4O_6(R\text{-ida})_4]^{4-}$ complex were unsuccessful. The mixed ligand complexes precipitated on the order of minutes from an acetonitrile solution of **1** containing greater than 4 equiv of the R-ida ligand. Ligand substitution in methanol, in which the starting material $[Mn_4O_6(bpea)_4]Br_4$ or **1** (the latter at much lower solubility) and complexes **8**−**11** are soluble gave a reddish solution upon addition of excess R-ida ligand within minutes, followed by gradual bleaching to a colorless solution and precipitation of flocculant material after about 10 h. It may be that the fully substituted product $[Mn_4O_6(R\text{-ida})_4]^{4-}$ is formed in methanol and that it is unstable.

Structures. The crystal structures of the full cation of **7** and the neutral complex **11** are shown in Figure 2, parts a and b, respectively. Figure 3 shows the $[Mn_4O_6]^{4+}$ cores only. The Mn and oxide O atoms in the crystal structures of **7** and **11** define the adamantane skeleton. The Mn atoms occupy the apexes of a tetrahedron and the O atoms occupy

(90) Basolo, F.; Pearson, R. G. *Mechanisms of Inorganic Reactions*, 2nd ed.; Wiley: New York, 1967.
(91) Zhang, L.; Shiping, Y.; Chunhui, L.; Daizheng, L.; Zonghui, J.; Cheng, P.; Wang, G.; Weng, L.; Xuebing, L. *J. Chem. Crystallogr.* **2000**, *30*, 251−254.
(92) Brewer, K. J.; Calvin, M.; Lumpkin, R. S.; Otvos, J. W.; Spreer, L. O. *Inorg. Chem.* **1989**, *28*, 4446−4451.
(93) Hagen, K. S.; Armstrong, W. H.; Hope, H. *Inorg. Chem.* **1988**, *27*, 7−969.
(94) Murahashi, S.-I. *Angew. Chem., Int. Ed. Engl.* **1995**, *34*, 2443−2465.
(95) Sheldon, R. A.; Kochi, J. K., *Metal-Catalyzed Oxidations of Organic Compounds*; Academic: New York, 1981.
(96) Meunier, B. *Biomimetic Oxidations Catalyzed by Transition Metal Complexes*; Imperial College Press: London, 2000; p 696.
(97) Jain, S. L.; Sain, B. *Angew. Chem., Int. Ed.* **2003**, *42*, 1265−1267.
(98) Murahashi, S.-I.; Komiya, N.; Terai, H.; Nakae, T. *J. Am. Chem. Soc.* **2003**, *125*, 15312−15313.
(99) Caudle, M. T.; Pecoraro, V. L. *Inorg. Chem.* **2000**, *39*, 5831−5837.

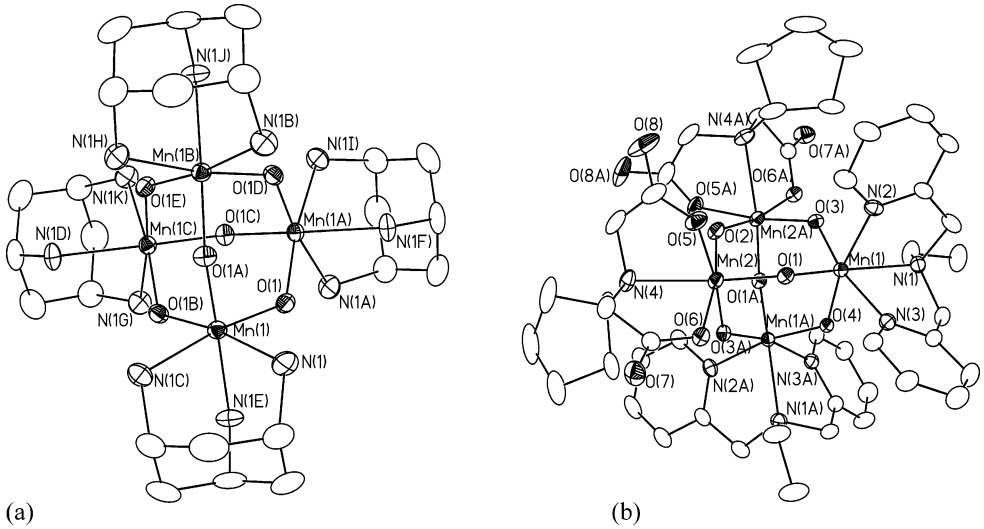

Figure 2. ORTEP plots of the structures and atom labeling schemes of (a) **7**$(ClO_4)_4$ and (b) **11** showing 30% probability thermal ellipsoids. Hydrogen atoms (and perchlorate counterions for **7**) are omitted for clarity.

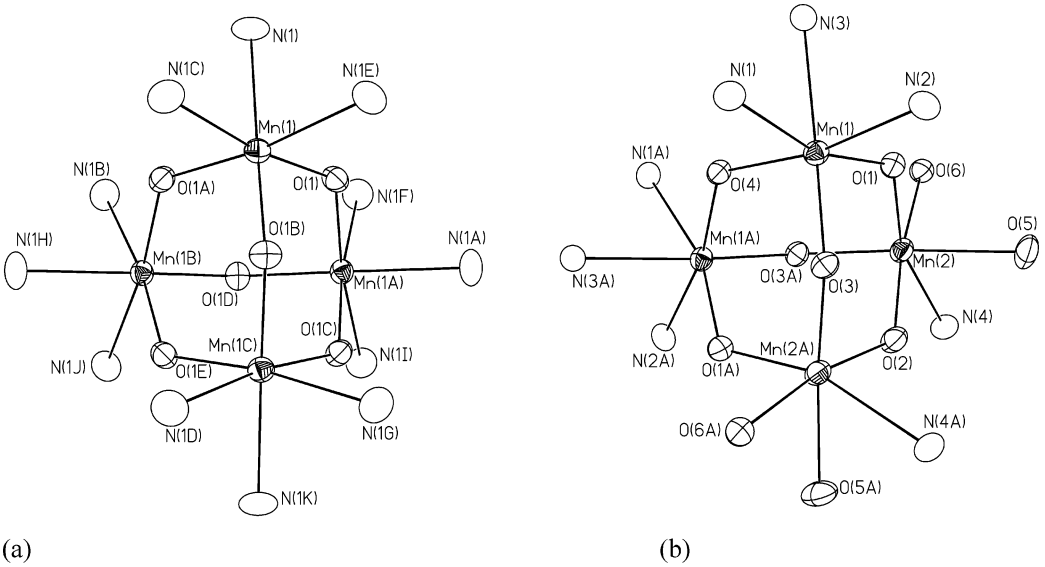

Figure 3. ORTEP plots of the $\{Mn_4O_6\}$ cores of (a) **7** and (b) **11** showing 30% probability thermal ellipsoids. Carbon and hydrogen atoms (and perchlorate counterions for **7**) are omitted for clarity.

Table 3. Selected Bonds Distances (Å) and Angles (deg) for $[Mn_4O_6(tach)_4](ClO_4)_4 \cdot 3CH_3CN \cdot 4.5H_2O$

bond distances		bond angles	
Mn(1)−O(1)	1.808(3)		
Mn(1)−N(1)	2.096(7)	O(1A)−Mn(1)−O(1)	98.0(2)
N(1)−C(1)	1.486(11)		
C(2)−C(1)	1.493(8)	Mn(1)−O(1)−Mn(1A)	129.3(4)

the apexes of an octahedron. Each Mn atom is coordinated to three bridging oxide O atoms and three atoms from the terminal ligands in pseudo-octahedral geometry. Complex **7** exhibits crystallographically imposed T_d point symmetry, rendering all the Mn atoms, bond lengths, and bond angles equivalent. The $Mn-O_{oxo}$ bond length of 1.808(3) Å and the Mn−O−Mn angle of 129.3(4)° for **7** (Table 3) are similar to those of **4** [1.796(1) Å and 128.0(1)°, respectively][20] and are generally consistent with metric data for other $Mn^{IV}-O_{oxo}$ complexes. The tach ligand displays local 3-fold symmetric coordination to the manganese ions in **7**, with a Mn−N distance of 2.101(6) Å, very similar to the average tacn Mn−N distance of 2.092(1) Å for **4** and significantly shorter than the $Mn-N_{alkyl}$ bond length of 2.196(2) Å for the bpea ligand of **1**.

In contrast to the high point symmetry of **7**, **11** exhibits only C_2 point symmetry. This symmetry results in four types of bridging oxo ligands, two of which lie along the crystallographic C_2 axis [O(2) and O(4) in Figure 3b]. Oxo bridge O(2) is trans to the carboxylate oxygen atoms of the ^{c}pent-ida ligands and has a Mn−O bond length of 1.7986(17) Å. Its Mn−O−Mn angle of 133.5(2)° (Table 4) is the largest angle measured thus far for a Mn−oxo adamantane shaped core. Oxo bridge O(4) is trans to two pyridyl nitrogen atoms of the bpea ligands and has a Mn−O bond length of 1.798(2) Å and a Mn−O−Mn angle of 127.2(2)°.

Of the four oxo bridges lying in the plane perpendicular to the C_2 axis, two [O(1) and O(1A)] are trans to a bpea tertiary amine nitrogen atom and a ^{c}pent-ida tertiary amine nitrogen atom, with a Mn−O−Mn angle of 127.95(16)° and

Table 4. Selected Bonds Distances (Å) and Angles (deg) for $[Mn_4O_6(bpea)_2(^c pent\text{-}ida)_2]\cdot 7MeOH$

bond distances		bond angles	
Mn(1)−O(1)	1.780(3)	O(1)−Mn(1)−O(3)	100.30(13)
Mn(1)−O(3)	1.792(3)	O(1)−Mn(1)−O(4)	98.51(12)
Mn(1)−O(4)	1.7980(18)	O(3)−Mn(1)−O(4)	98.14(11)
Mn(1)−Mn(2)	3.2114(10)	O(1)−Mn(2)−O(3A)	97.19(13)
Mn(1)−Mn(1A)	3.2207(13)	O(1)−Mn(2)−O(2)	98.47(12)
Mn(2)−O(1)	1.794(3)	O(3A)−Mn(2)−O(2)	94.08(12)
Mn(2)−O(3A)	1.798(3)	O(1)−Mn(2)−O(5)	89.43(14)
Mn(2)−O(2)	1.7986(17)	O(3A)−Mn(2)−O(5)	172.69(14)
O(2)−Mn(2A)	1.7986(17)	O(2)−Mn(2)−O(5)	87.98(13)
O(3)−Mn(2A)	1.798(3)	O(1)−Mn(2)−O(6)	90.33(12)
O(4)−Mn(1A)	1.7980(18)	O(3A)−Mn(2)−O(6)	90.01(12)
		O(2)−Mn(2)−O(6)	169.75(14)
		O(5)−Mn(2)−O(6)	86.84(13)
		Mn(2A)−O(2)−Mn(2)	133.5(2)
		Mn(1)−O(3)−Mn(2A)	130.36(17)
		Mn(1)−O(4)−Mn(1A)	127.2(2)
		Mn(1)−O(1)−Mn(2)	127.95(16)

a Mn−O bond length of 1.780(2) Å. The remaining two bridges [O(3) and O(3A)] are trans to a pyridyl nitrogen atom and a carboxylate oxygen atom of bpea and ^{c}pent-ida ligands, respectively, with a Mn−O−Mn angle of 130.36(17)° and an average Mn−O bond length of 1.792(2) Å. All of these bond lengths are comparable to those of **1**, which is characterized by four Mn−O bonds 1.806(1) Å long and two Mn−O bonds 1.786(2) Å long.

The Mn−N bond lengths of the bpea ligands of **11** are similar to those of **1**: an average Mn−N_{alkyl} bond length of 2.173(4) Å and two kinds of Mn−N_{py} bonds, a "short" Mn−N_{py} bond with an average length of 2.080(4) Å and a slightly longer Mn−N_{py} bond with an average length of 2.094(3) Å. Longer Mn−N_{alkyl} bonds[100] are observed for other structurally characterized compounds whose multidentate ligands are comprised of both alkyl and pyridyl nitrogen atoms, including bpea,[65,66,68] bpta,[68] bispicen,[101,102] and tmpa.[103] The four carboxylate Mn−O bonds of the ^{c}pent-ida ligand of **11** [average length of 2.024(3) Å] are somewhat longer than similar Mn^{IV}−O bonds for other terminal carboxylate ligand Mn complexes (1.980−1.999 Å).[104−106]

The average Mn···Mn distance of **11** [3.2161(11) Å] is somewhat shorter than the corresponding distance in **4** [3.227(2) Å], **7** (3.269 Å), and **1** [3.248(1) Å].

Physical Properties. Mass Spectrometry. Electrospray ionization mass spectrometry data are summarized in Table S2 and all spectra can be found in the Supporting Information. The ESI mass spectra of **7** and **8** are shown in Figures 4 and 5, respectively.

The substitution products can be divided into two groups: the cations and the neutral species. The $[Mn_4O_6]^{4+}$ cations readily lose an anion to form $[M - ClO_4]^+$ species. The tach

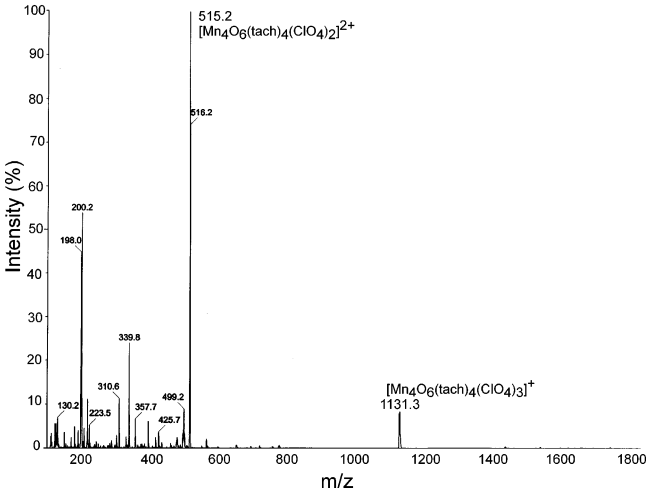

Figure 4. Positive ion electrospray ionization mass spectrum of **7** in acetonitrile at unit resolution.

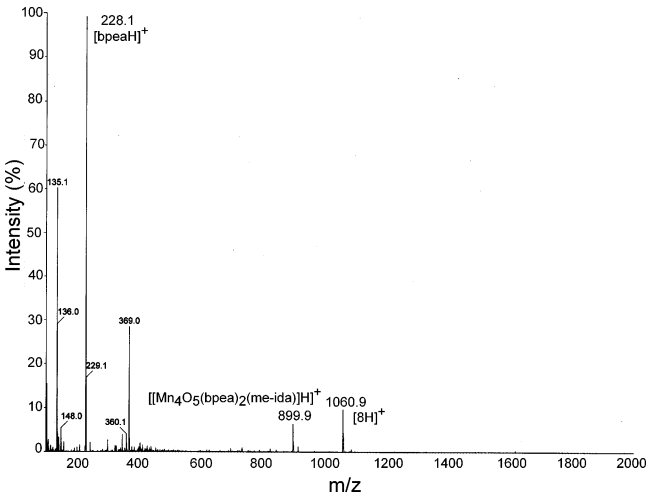

Figure 5. Positive ion electrospray ionization mass spectrum of **8** in water/methanol (10%) at unit resolution.

(**7**) and tacn (**4**) complexes behave similarly, with $[M - ClO_4]^+$ and $[M - 2ClO_4]^{2+}$ being the predominant species, but otherwise exhibiting very little fragmentation. The mass spectrum of complex **6** shows striking similarity to those of the strong amine donor ligand complexes **4** and **7**, with major peaks at $[M - ClO_4]^+$ (1082.9), $[M - 2ClO_4]^{2+}$ (491.7), $[M - 3ClO_4]^{3+}$ (294.6), and $[M - 4ClO_4]^{4+}$ (196.1). The mass spectrum for the mixed dien/bpea complex (**5**), with a major peak at $[M - ClO_4]^+$ (1275.2), showed similar behavior to that of **1**, which exhibited a much greater tendency toward core fragmentation in the gas phase.[21]

The mass spectra of the $[Mn_4O_6(bpea)_2(R\text{-}ida)_2]$ complexes are similar to each other, exhibiting prominent species at $[M + H]^+$ (1060.9, 1213.4, 1145.4, and 1169.5 for **8**, **9**, **10**, and **11**, respectively) and $[M + Na]^+$ (1235.4, 1167.3, and 1191.4 for **9**, **10**, and **11**, respectively), as well as prominent peaks that correspond to addition of R-ida^{2-} ligands and peaks corresponding to loss of CO_2.

Electronic and Vibrational Spectroscopy. The IR spectra of the $[Mn_4O_6]^{4+}$ cores show a number of bands attributable to the different ligands and the ClO_4^- anion (∼1119 and

(100) The comparison is among Mn^{IV}−N_{alkyl} and Mn^{IV}−N_{py}, which are trans to μ-O ligands.
(101) Collins, M. A.; Hodgson, D. J.; Michelson, K.; Towle, D. K. *J. Chem. Soc., Chem. Commun.* **1987**, 1659−1660.
(102) Goodson, P. A.; Glerup, J.; Hodgson, D. J.; Michelsen, K.; Pedersen, E. *Inorg. Chem.* **1990**, *29*, 503−508.
(103) Towle, D. K.; Botsford, C. A.; Hodgson, D. *Inorg. Chim. Acta* **1988**, *141*, 167−168.
(104) Suzuki, M.; Senda, H.; Kobayashi, Y.; Oshio, H.; Uehara, A. *Chem. Lett.* **1988**, 1763−1766.
(105) Gohdes, J. W. Ph.D. dissertation, University of California, Berkeley, 1991.
(106) Bhaduri, S.; Pink, M.; Christou, G. *Chem. Commun.* **2002**, 2352−2353.

625 cm^{-1}),[107] and each compound also exhibits intense bands attributed to the Mn−O−Mn stretch in the region between about 695 and 732 cm^{-1} (Table S3).[21,22] An intense band for **1** at 708 cm^{-1} is near the middle of this range, while the corresponding bands for the substitution products **4** (732 cm^{-1}) and **10** (695 cm^{-1}) delineate the extremes.

The mixed ligand R-ida series also display two intense bands around 1620 and 1380 cm^{-1} attributed to the coordinated carboxylate ligand.[107] The mode of coordination of R-ida is readily determined from the values of ν_a(COO) and ν_s(COO) and the value of $\Delta = [\nu_a(\mathrm{COO}) - \nu_s(\mathrm{COO})]$.[107,108] The infrared spectra of the $[Mn_4O_6(bpea)_2(R\text{-}ida)_2]$ series all have a value of Δ between 240 and 244 cm^{-1}, which is characteristic of unidentate coordination of the carboxylate ion. As anticipated, unidentate coordination of the carboxylate moieties of the ^{c}pent-ida ligand to the Mn ions has been verified for **11** by X-ray structural analysis, substantiating the structurally characterized sample as representative of the bulk material. A survey of representative metalloprotein crystal structure determinations[109] reveals that unidentate carboxylate can bind either syn or anti with respect to the lone pairs of electrons. As expected, ^{c}pent-ida ligation to the Mn ion is anti unidentate.

The electronic spectra of all the complexes are similar to each other, with the most notable feature in the absorption spectrum being the putative $O\rightarrow Mn^{IV}d\pi^*$ charge-transfer band in the range 546 to 591 nm, as well as a number of less intense bands at 990−1000 nm for all of the complexes, most likely d−d transitions (Table S3). The fully substituted strong N-donor ligand complexes (**4**, **6**, and **7**) also exhibit a very weak shoulder at about 750 nm.

Electrochemistry. The ligands described here stabilize the adamantane-shaped $[Mn_4O_6]$ core in the $Mn^{III}(Mn^{IV})_3$, $(Mn^{IV})_4$, and $Mn^{V}(Mn^{IV})_3$ oxidation states. Ligand substitution on **1** greatly decreased the reduction potential of the (IV, IV, IV, IV)/(III, IV, IV, IV) redox couple from $E_{1/2} = -0.28$ to -1.03 V for **9**, a shift of 750 mV. Cyclic voltammograms of **7** and **9** are shown in Figures 6 and 7, respectively, and all electrochemical data are summarized in Table S3.

Particularly noteworthy is the substantial inductive effect of the substituted iminodicarboxylates, as shown in the plot of $O\rightarrow Mn^{IV}d\pi^*$ LMCT energy versus $E_{1/2}$ (Figure 8). Figure 8 also illustrates the differentiation of the strong σ-donor amines and the strong π-donor carboxylates with respect to LMCT. Tuning of the redox potentials of the $[Mn_4O_6]^{4+}$ complexes follows a ranking of the ancillary ligands, as determined for a number of mononuclear ruthenium and dinuclear manganese complexes, based on their redox potentials: $RO^- > RCO_2^- > R_3N > R_2NH >$ pyridine.[110−113]

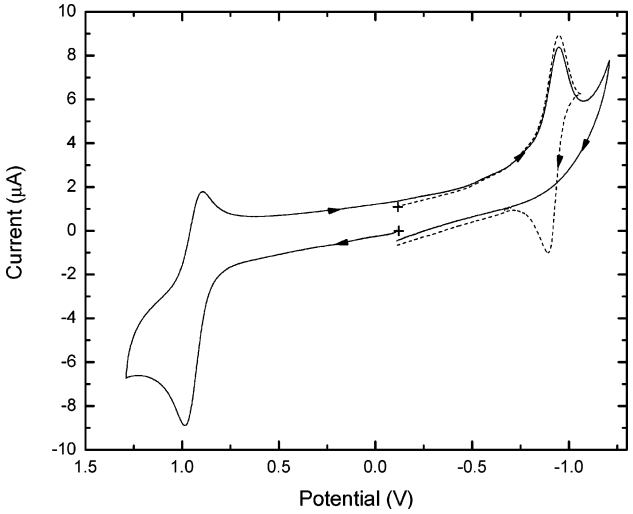

Figure 6. Cyclic voltammograms of an acetonitrile solution 1.20 mM in **7**$(ClO_4)_4$ and 0.2 M in TBAP illustrating quasireversible oxidation and reduction. The two scans have the same starting potential (denoted with +) but differ by scan direction and scan window. Potentials are versus Fc/Fc^+.

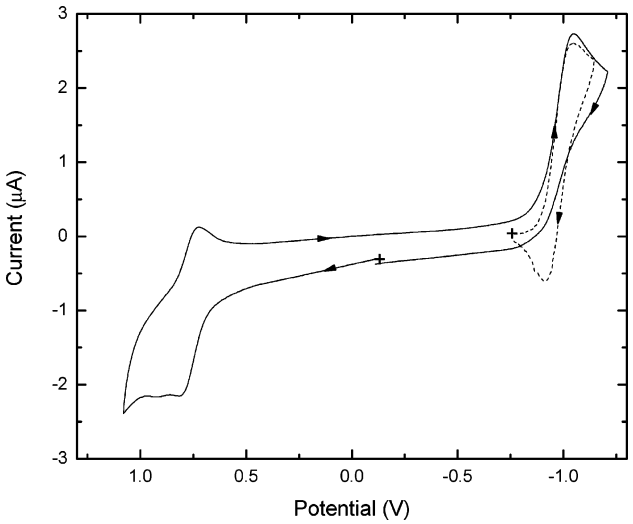

Figure 7. Cyclic voltammograms of a propylene carbonate solution 290 μM in **9** and 0.2 M in TBAP illustrating quasireversible oxidation and reduction. The two scans differ by starting potential (denoted with +), scan direction and scan window. Potentials are versus Fc/Fc^+.

Importantly, substitution of bpea with strong donor ligands also affords ready access to the $Mn^{V}(Mn^{IV})_3$ oxidation state. Complexes **4**, **7**, **9**, **10**, and **11** exhibit quasireversible CV for the (V, IV, IV, IV)/(IV, IV, IV, IV) redox couple ($E_{1/2}$ of 0.978, 0.942, 0.775, 0.718, and 0.641 V, respectively), with the R-ida complex **11** having the lowest (V, IV, IV, IV)/(IV, IV, IV, IV) redox couple of the known adamantane-shaped $[Mn_4O_6]^{4+}$ complexes. Synthesis, characterization, and reactivity of manganese−oxo complexes in the $Mn^{V}(Mn^{IV})_3$ oxidation state figure prominently in modeling studies aimed at evaluating recent proposals for PSII-catalyzed water oxidation, in which a Mn^{V} intermediate is proposed for the O−O bond-forming step.[57−61,114] Furthermore, a $Mn^{V}(Mn^{IV})_3$ oxidation state has been proposed for the S_4 state of the Mn_4 OEC.[57, 63, 64]

(107) Nakamoto, K., *Infrared and Raman Data of Inorganic and Coordination Compounds*, 5 ed.; John Wiley: New York, 1997; Vols. A & B.
(108) Deacon, G. B.; Phillips, R. J. *Coord. Chem. Rev.* **1980**, *33*, 227−250.
(109) Rardin, R. L.; Tolman, W. B.; Lippard, S. J. *New J. Chem.* **1991**, *15*, 417−430.
(110) Lever, A. B. P. *Inorg. Chem.* **1990**, *29*, 1271−1285.
(111) Fielder, S. S.; Osborne, M. C.; Lever, A. B. P.; Pietro, W. J. *J. Am. Chem. Soc.* **1995**, *117*, 6990−6993.
(112) Thorp, H. H.; Brudvig, G. W. *New. J. Chem.* **1991**, *15*, 479−490.
(113) Manchanda, R.; Brudvig, G. W.; Crabtree, R. H. *Coord. Chem. Rev.* **1995**, *144*, 1−38.

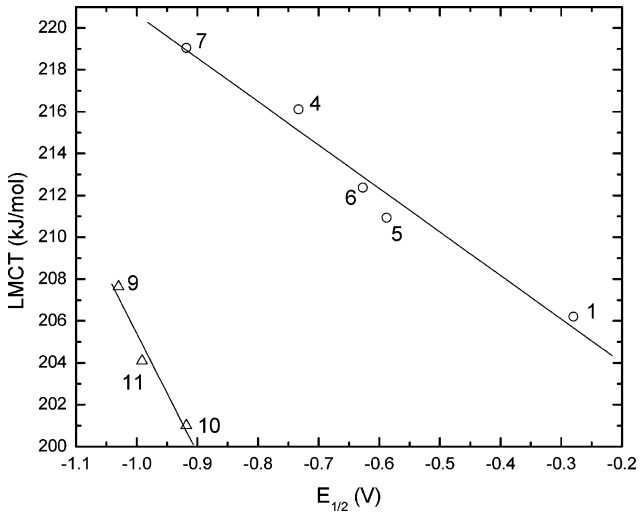

Figure 8. Plot of LMCT energy versus $E_{1/2}$ of the (III,IV,IV,IV)/(IV,-IV,IV,IV) redox couple. △ = iminodicarboxylates and ○ = amines. Potentials are versus Fc/Fc^+.

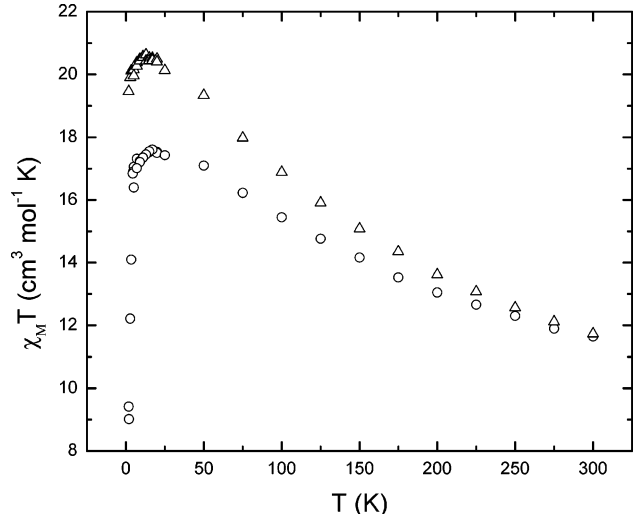

Figure 9. Temperature dependence of $\chi_M T$ of **7**$(ClO_4)_4$ (△) and **9** (○) at 0.5 T.

Magnetic Susceptibility and Isothermal Magnetization. Magnetic susceptibility measurements versus temperature were conducted on powdered samples of **4**, **7**, **8**, and **9** and isothermal magnetization versus applied magnetic field were measured for **1**, **7**, and **9**.

Magnetic susceptibility data for **7** and **9** are plotted as $\chi_M T$ versus T in Figure 9. Data for **4** and **8** are in Supporting Information as Figures S7 and S8, respectively. Qualitatively, the behavior for adamantane complexes synthesized via ligand substitution is similar to that observed for **1**.[21,23] Each complex is overall ferromagnetically coupled, with room temperature (300 K) $\chi_M T$ values between 10.9 and 12.3 cm^3 mol^{-1} K.[115] These values are also similar to the room temperature $\chi_M T$ value for **1** of 10.9. Overall ferromagnetic coupling within **4** has been reported previously.[19,20] Upon cooling, the value of $\chi_M T$ increases to a maximum in the vicinity 7−20 K, below which temperature the value decreases. Notable are the maximum $\chi_M T$ values for **4** and **7** at 0.5 T of 20.5 (7 K) and 20.6 (13 K), respectively, which are very close to the value expected for an S = 6 ground state of 21.0. It is expected, however, that significant changes in the ligand field environment of the Mn^{IV} ions with ligand substitution, as well as changes in the magnetic exchange pathways due to $[Mn_4O_6]^{4+}$ core structural differences for the complexes discussed above might well lead to differences in magnetic exchange and ground-state spin. For example, the values of maximum $\chi_M T$ were highest for the highest symmetry complexes **4** and **7**, somewhat lower for **1** (18.3 at 18 K), and lowest for the mixed ligand complexes **8** and **9** at 17.5 (20 K) and 17.6 (17 K), respectively. Further indications of the differences in the magnetic behavior among these complexes are evident in the variable-field magnetization and analysis of the magnetic susceptibility as a function of temperature.

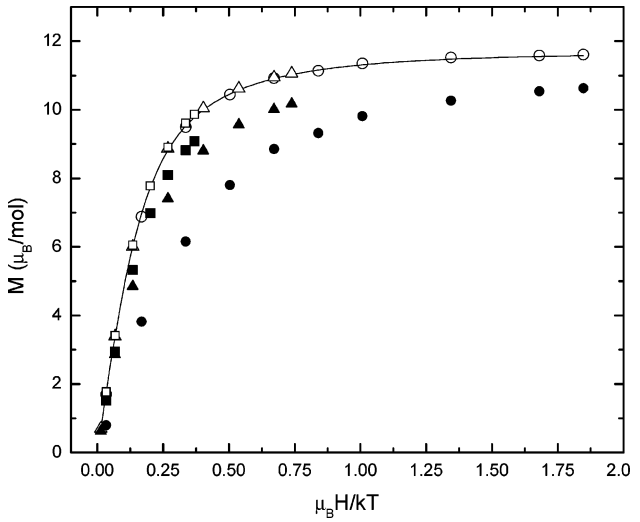

Figure 10. Isothermal magnetization of **7** (○, △, □) and **9** (●, ▲, ■). The solid line corresponds to a fit of the Brillouin function for **7**$(ClO_4)_4$ (2 K data) with $S = 6$ and $g = 1.94$. Symbols: 2 K (○, ●), 5 K (△, ▲), 10 K (□, ■).

The ground-state spin of each **1**, **7**, and **9** was studied with isothermal magnetization. The field dependence of the magnetization of **7** at 2, 5, and 10 K, as a plot of M (μ_B/mol) versus $\mu_B H/kT$ (Figure 10), exhibits saturation around 11.6 μ_B/mol, which could be fit with the Brillouin function with $S = 6$ and $g = 1.94$.[116] For comparison, analysis of the magnetic behavior of **4** previously established that it has an $S = 6$ ground state.[19, 20]

On the other hand, the magnetization behavior of **9**, which exhibited saturation around 10.6 μ_B/mol (Figure 10), suggests population of low lying ($S < 6$) states and zero-field splitting of the ground state. The magnetization behavior of **1** (Figure S9) also indicates some degree of zero-field splitting in the ground state.

In prior work, the magnetic susceptibility as a function of temperature for **4** was modeled with the Van Vleck equation[117] using an isotropic Heisenberg exchange Hamiltonian

(114) Limburg, J.; Szalai, V. A.; Brudvig, G. W. *J. Chem. Soc., Dalton Trans.* **1999**, 1353−1362.

(115) For comparison, the spin-only $\chi_M T$ value for four uncoupled high-spin d^3 ions is 7.50 cm^3 mol^{-1} K.

(116) When H/kT is large, the magnetization M (in units of μ_B/mol) saturates at a value given by gS.

in the form $\hat{\mathbf{H}} = -Jij\hat{\mathbf{S}}_\mathbf{i}\cdot\hat{\mathbf{S}}_\mathbf{j}$ with a single J (14.5 cm^{-1}), based on an idealized tetrahedral symmetry.[20] The quality of the fit, which was relatively poor, was significantly improved with incorporation of a large biquadratic exchange term j (J = 13.8 cm^{-1}, j = 7.8 cm^{-1}). On the other hand, the ferromagnetic exchange of **1**, possessing two different types of oxo bridges coupling the Mn^{IV} ions,[21] was modeled with $\hat{\mathbf{H}} = -J_{ij}\hat{\mathbf{S}}_\mathbf{i}\cdot\hat{\mathbf{S}}_\mathbf{j}$ using two exchange constants, giving an excellent fit with J_1=10.2 cm^{-1}, J_2=90.0 cm^{-1}, and g = 1.88.[23] A biquadratic exchange term did not improve the quality of the fit markedly. While we have not found a single magnetic exchange model that adequately describes the magnetic behavior of all of the adamantane-shaped $[Mn_4O_6]^{4+}$ complexes, the overall ferromagnetic coupling of the Mn^{IV} ions is best regarded as pairwise ferromagnetic. The overall ferromagnetic coupling in these $[Mn_4O_6]^{4+}$ cores is unusual among the known tetranuclear manganese−oxo aggregates,[37,40,42,45,118−124] and is the subject of an ongoing investigation that incorporates broken symmetry/density functional theory (BS/DFT) to model the magnetic exchange.[125]

^{1}H NMR Spectroscopy. The ^{1}H NMR spectra of **4**−**11** can be understood in terms of their magnetic properties and assuming that the solution structural symmetry is the same as that displayed in the solid state. The ^{1}H NMR spectra of **1**, **7**, **10**, and **11** (Figure 11) are representative of the differences observed for the various types of ligands. ^{1}H NMR spectra of the remaining complexes can be found in the Supporting Information. Much of the analysis presented here has benefited from earlier research on paramagnetic ^{1}H NMR properties of manganese−oxo complexes.[21,25,126,127]

Ligand proton resonances can be separated into two types, those assigned to pyridyl ring protons and those assigned to methylene protons. Proton resonances for the complexes described here are found in the range $+60 > \delta > -152$ ppm and are provided in Table S4. The pyridyl ring proton resonances for **1** are found in the region $+55 > \delta > -20$ ppm, and the methylene groups of **1** fall in the range $-22 > \delta > -82$ ppm.[21]

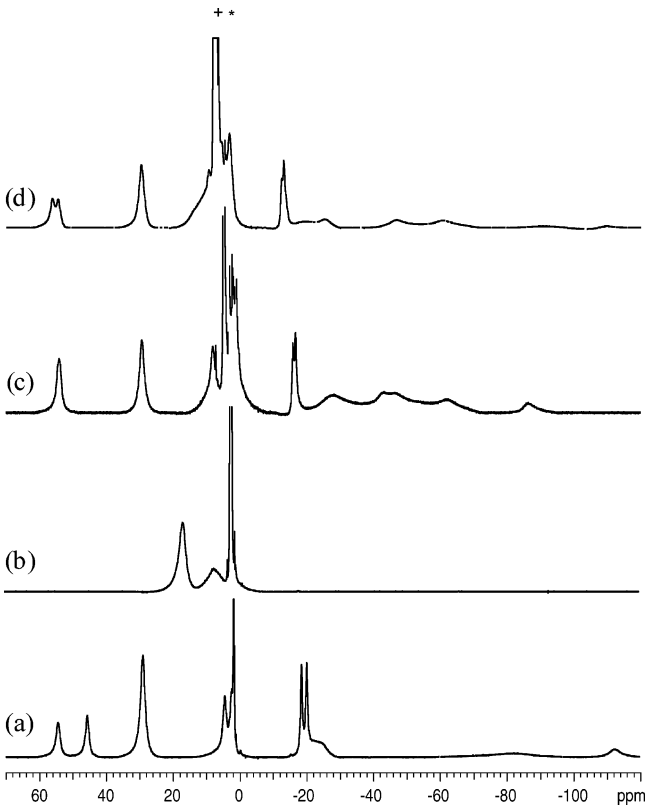

Figure 11. ^{1}H NMR spectra of (a) **1**, (b) **7**, (c) **10**, and (d) **11**. Conditions: CD_3CN (**1** and **7**), CD_3OD (**10** and **11**). *, CD_2HCN; +, CD_2HOD.

While the methylene resonances for **4** are at −41.4 ppm (2900 Hz) and −56.7 ppm (1640 Hz), and the methylene resonances of the Medien complex **6** comprise overlapping peaks centered at −45 ppm (3800 Hz), the methylene resonances of the tach complex **7** are downfield at 16.8 ppm (703 Hz) and 7.2 ppm (1640 Hz). The methylene protons of **7** are shifted downfield because they are further removed from the metal center by one additional σ-bond. The methine protons of the tach ligand are not observed for **7**. The two equal-intensity resonances for both **4** and **7** are distinguished by measurably different peak widths. The broader resonances are assigned to those methylene protons directed toward the metal center (axial, H_{ax}), while the sharper resonances are assigned to those methylene protons directed away from the metal center (equatorial, H_{eq}), analogous to the assignments made for the methylene protons of $[Mn_2O(OAc)_2(tacn)_2]^{2+}$.[126]

The bpea/R-ida mixed ligand complexes exhibit new resonances in the region $-50 > \delta > -100$ ppm, corresponding to the methylene protons of the R-ida ligands. Additional resonances of some of the alkyl nitrogen substituents are evident in the region $8 > \delta > -1$ ppm. Although the bpea ligands within each of these complexes are equivalent, we did note differences in the split (or lack thereof) of the 4,4′ and 5,5′ pyridyl ring proton resonances between the complexes.[128] For example, the 5,5′ pyridyl ring proton resonances of **8** and **10** are overlapping at 300 MHz

(117) Carlin, R. L. *Magnetochemistry*; Springer-Verlag: Berlin, 1986; p 15−18.
(118) Mikuriya, M.; Yamato, Y.; Tokii, T. *Chem. Lett.* **1991**, *8*, 1429−1432.
(119) Chandra, S. K.; Chakravorty, A. *Inorg. Chem.* **1991**, *30*, 3795−.
(120) Aubin, S. M. J.; Dilley, N. R.; Wemple, M. W.; Maple, M. B.; Christou, G.; Hendrickson, D. N. *J. Am. Chem. Soc.* **1998**, *120*, 839−840.
(121) Chan, M. K.; Armstrong, W. H. *J. Am. Chem. Soc.* **1989**, *111*, 9121−9122.
(122) Chan, M. K.; Armstrong, W. H. *J. Am. Chem. Soc.* **1990**, *112*, 4985−4986.
(123) Suzuki, M.; Hayashi, Y.; Munezawa, K.; Suenaga, M.; Senda, H.; Uehara, A. *Chem. Lett.* **1991**, 1929−1932.
(124) Afrati, T.; Dendrinou-Samara, C.; Raptopoulou, C. P.; Terzis, A.; Tangoulis, V.; Kessissoglou, D. P. *Angew. Chem., Int. Ed.* **2002**, *41*, 2148−2150.
(125) Armstrong, W. H.; Dubé, C. E.; Gatteschi, D.; Sessoli, R.; Totti, F.; Noodleman, L. In *Magnetic coupling in and reactivity of multinuclear manganese(IV) compounds: Insight from density functional theory*, 220th ACS National Meeting, Washington, DC, Aug. 20−24, 2000; American Chemical Society: Washington, DC, 2000.
(126) Wright, D. W.; Mok, H. J.; Dubé, C. E.; Armstrong, W. H. *Inorg. Chem.* **1998**, *37*, 3714−3718.
(127) Mok, H. J. Ph.D., Boston College, Chestnut Hill, MA, 1999.
(128) No definitive assignment was made for the 3,3′ pyridyl ring proton resonances of the bpea/R-ida mixed ligand complexes. See: *J. Am. Chem. Soc.* **1998**, *120*, 3704−3716 for a tabulation of assignments for the 3,3′ pyridyl ring proton resonances of related complexes.

(52.0 and 54.7 ppm, respectively), while the splitting of the 4,4′ pyridyl ring proton resonances, at −17.0 and −17.3 ppm for **8** and −16.0 and −16.7 for **10**, is 0.3 and 0.7 ppm, respectively. On the other hand, the 5,5′ pyridyl ring proton resonances of **11** exhibit a slight split (55.6, 53.8 ppm, Δ = 1.8 ppm), while the splitting of the 4,4′ pyridyl ring proton resonances (−16.7, −17.3 ppm, Δ = 0.6 ppm) is similar to that of **8** and **10**. These data are in contrast to the larger separations of the 4,4′ (−18.6, −20.2 ppm, Δ = 1.6 ppm) and 5,5′ (54.9, 46.1 ppm, Δ = 8.8 ppm) pyridyl ring proton resonances of **1**. Previously, we had suggested that the differences in the pyridyl ring proton resonances of **1** were due to longer and shorter Mn−N_{pyr} bonds, the shorter bond leading to tighter coupling to the core and a larger chemical shift.[21] Comparison of the two Mn−N_{pyr} bonds, 2.090(2) and 2.108(2) Å for **1** (longer − shorter Δ = 0.018 Å) and 2.079(4) and 2.094(4) Å for **11** (Δ = 0.015 Å) shows a similarity of the longer−shorter difference, suggesting that the differences in the 5,5′ and 4,4′ pyridyl ring proton resonances are due to some other factor. An implication of this result is that although the contact shift of the pyridyl ring proton resonances is likely the dominant component of their isotropic shift, they may have a measurable dipolar component.

Protonation Studies. We have reported structural and electronic changes concomitant with changes in the protonation state of the oxo bridges of **1** and **4**.[20,21,25] Ligand substitution with iminodicarboxylate ligands greatly increased the overall electron density of the $[Mn_4O_6]^{4+}$ cores, as demonstrated by the large shift in reduction potentials of **8**−**11**. Furthermore, the lower symmetry of the aforementioned complexes creates four site-differentiated oxo bridges, compared with two site-differentiated bridging oxo ligands for **1**. Unlike the subtle oxo bridge site differentiation of **1**, however, we expected that the substantial inductive effect of the carboxylate ligands would significantly differentiate oxo bridge electron densities of **8**−**11**. In addition, we anticipated that the increased overall electron density of the $[Mn_4O_6]^{4+}$ core would facilitate protonation in water, unlike protonation of **1**, which required a strong acid in acetonitrile.

Reversible protonation of an oxo bridge of **8** in water with $HClO_4$ to give $[Mn_4O_5(OH)(bpea)_2(me\text{-}ida)_2](ClO_4)$ (**8**H(ClO_4)) was demonstrated spectrophotometrically (Figure 12) and by ^{1}H NMR in D_2O using CF_3SO_3H to give **8**H(CF_3SO_3) (Figure 13) (see also the ESI mass spectrum of **8**, Figure 5).

Formation of $\mathbf{8}H^+$ was complete after addition of 1 equiv of acid. The observation of distinct ^{1}H NMR spectra for **8** and **8**H(CF_3SO_3) in the course of titration of **8** with CF_3SO_3H is a consequence of the slow rate of proton self-exchange on the NMR time scale and is consistent with data for other metal−oxo complexes.[21,25,129−132] The effective

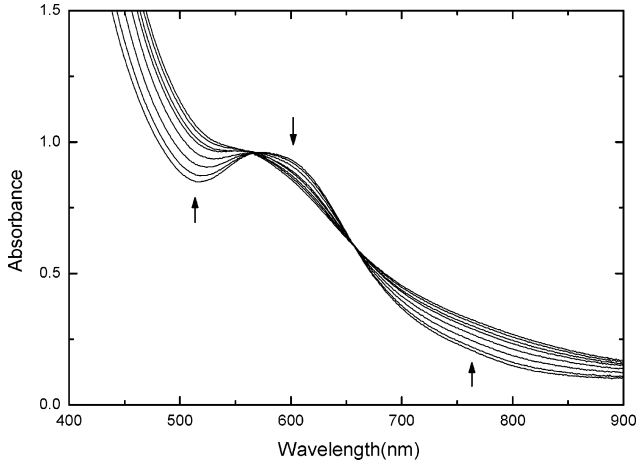

Figure 12. Spectrophotometric titration of an aqueous solution of **8** with $HClO_4$ (isosbestic points at 567 and 657 nm). See the Experimental Section for details.

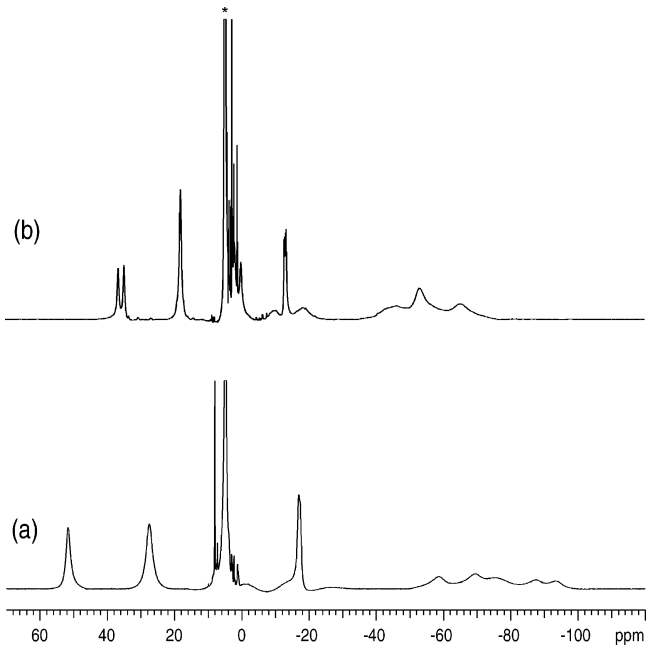

Figure 13. ^{1}H NMR of (a) **8** and (b) **8** plus 1 equiv of CF_3SO_3H in D_2O to form **8**H(CF_3SO_3). See the Experimental Section for details. *, HOD.

aqueous pK_a of **8** of 2.20 ± 0.03, determined spectrophotometrically with $HClO_4$ using eq 1 (Figure S14), is among the highest pK_a values of the adamantane-like $[Mn_4O_6]^{4+}$ cores, as expected for the iminodicarboxylate ligand me-ida. Protonation of **8** was also demonstrated with CF_3COOH and CH_3SO_3H, giving an aqueous pK_a of 2.07 and 2.00, respectively. Quantitative reversibility of protonation was verified by spectrophotometric back-titration with Et_3N.

Protonation of **11** in water with $HClO_4$ and CF_3SO_3H was followed spectrophotometrically as well, and fitting of absorbance versus pH for titration with $HClO_4$ (Figure S15) gave an aqueous pK_a of 2.32 ± 0.02. Ligand electronic effects on the adamantane-shaped $[Mn_4O_6]^{4+}$ core tune the oxo bridge acidity over 11 orders of magnitude.[133] Ligand tuning of the manganese−oxo core effective acidity has also

(129) Kramarz, K. W.; Norton, J. R., Progress in Inorganic Chemistry. In *Progress in Inorganic Chemistry*; Karlin, K. D., Ed.; Wiley: New York, 1994; Vol. 42, pp 1−65.
(130) Carroll, J. M.; Norton, J. R. *J. Am. Chem. Soc.* **1992**, *114*, 8744−8745.
(131) Fox, S.; Alaganandan, N.; Marten, W.; Karlin, K. D.; Blackburn, N. J. *J. Am. Chem. Soc.* **1996**, *118*, 24−34.
(132) Evans, D. R.; Mathur, R. S.; Heerwegh, K.; Reed, C. A.; Xie, Z. *Angew. Chem., Int. Ed. Engl.* **1997**, *36*, 1335−1337.

Table 5. Comparison of Reduction Potentials and Acid Dissociation Constants for **1**, **4**, and **11** with Selected $[Mn_2O_2(X\text{-salpn})_2]$ Complexes

$[Mn_4O_6]^{4+}$			$[Mn_2O_2]^{4+}$ [a]		
	$E_{1/2}$ (mV)[c]	pK_a (H_2O)		$E_{1/2}$ (mV)[c]	pK_a (H_2O)
1	−280	−6.5[d]	**14**[b]	−440	−0.7[d]
4	−733	3.10	**15**[b]	−795	4.0[d]
11	−991	2.32	**16**[b]	−1048	6.6[d]

[a] $[Mn_2O_2]^{4+}$ data from Baldwin et al.[134] [b] $[Mn_2O_2(5\text{-}NO_2\text{-salpn})_2]$ (**14**); $[Mn_2O_2(5\text{-Cl-salpn})_2]$ (**15**); $[Mn_2O_2(5\text{-}OCH_3\text{-salpn})_2]$ (**16**); X-salpn are derivatives of H_2salpn (*N*,*N*′-trimethylenebis(salicylidene)-1,3-diaminopropane) with substitution on the phenolate rings. [c] $E_{1/2}$ versus Fc/Fc^+; data for **14**, **15**, and **16** corrected to Fc/Fc^+ using $E_{1/2}$ (Fc/Fc^+) = 460 mV versus the SCE in CH_2Cl_2 with $[Bu_4N][PF_6]$ electrolyte.[73] [d] pK_a measured in acetonitrile. The aqueous pK_a was estimated using the relation pK_a(H_2O) = pK_a(CH_3CN) − 7.5[135]

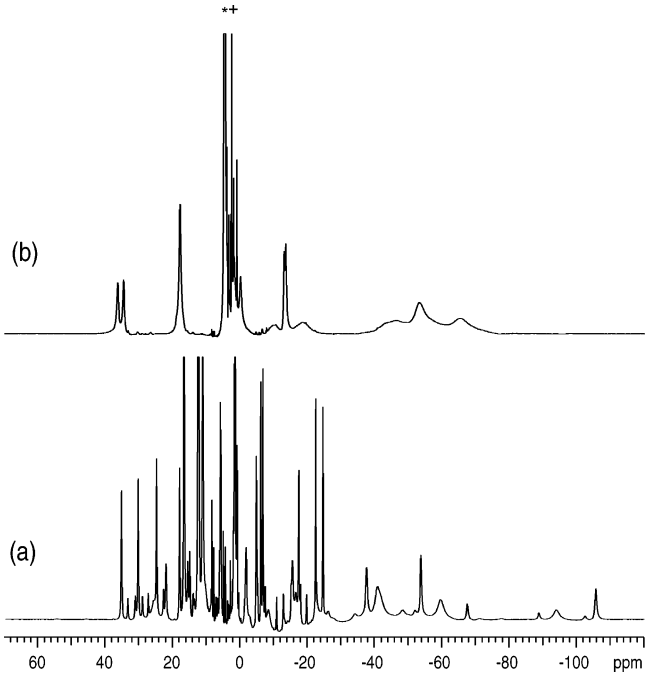

Figure 14. ^{1}H NMR of (a) **1**H$(CF_3SO_3)_5$ in CD_3CN and (b) **8**H(CF_3SO_3) in D_2O. *, HOD; +, CD_2HCN.

been demonstrated for the dimeric Mn^{IV} series $[Mn_2(\mu\text{-}O)_2(X\text{-salpn})_2]$, whose oxo bridge aqueous pK_a values ranged from −0.7 to 6.6 (Table 5).[134]

Although the chemical shifts and line widths of the resonances of the protonated complex **8**H(CF_3SO_3) are qualitatively similar to protonation results observed for **1** in acetonitrile, there are some striking differences (Figure 14). Solution magnetic susceptibility measurements reveal that the magnetic coupling changes from overall ferromagnetic for **8** ($\chi_M T$ of 12.5 cm^3 mol^{-1} K) to overall moderate antiferromagentic for **8**H^+ (6.3 cm^3 mol^{-1} K)[115] following protonation with 1 equiv of CF_3SO_3H in D_2O, similar to the degree of change seen for protonation of **1**. However, while there are four site-differentiated oxo bridges in **8**, the solution structural symmetry of **8**H^+ reveals essentially a single protonation isomer, unlike the two protonation isomers observed for **1**H^+ by ^{1}H NMR, one for each of the site-differentiated oxo bridges in **1**.[21,136] Furthermore, **8**H^+ exhibits equivalency of the bpea ligands, similar to that observed for **8** (vide supra). The higher solution symmetry of **8**H^+ relative to that observed for **1**H^+ is consistent with protonation at one of the two oxo bridges on the C_2 axis. We would expect this to be the oxo bridge trans to two carboxylate ligands (atom O(2) in Figure 3), based on the significant donor strength of the carboxylate oxygen atoms.

About 30 min after addition of either CF_3SO_3H or $HClO_4$ to an aqueous solution of **8** or **11**, the protonated complex precipitated from solution. The precipitate of either **8**H^+ or **11**H^+ could be readily solubilized with Et_3N, however, affording the spectrum of **8** or **11**, with nearly quantitative recovery.

Concluding Remarks

Although the tetranuclear arrangement of Mn ions in adamantane-shaped $[Mn_4O_6]^{4+}$ is too symmetrical and the Mn···Mn distance too long for it to be considered as an accurate *structural* model of the S_0−S_2 states of the active site,[1−6,137] this core has *mechanistic* implications with regards to S-state advancement and substrate oxidation at the active site. For example, EXAFS analysis of the Mn−oxo core within PSII reveals a metal−metal distance increase observed for the PSII Mn_4 when advancing from S_2 to S_3 states,[48] suggesting to us that the Mn−oxo core may undergo significant structural rearrangement, rather than necessarily an increase in the Mn−O_{oxo} bond length. We believe a core "shape-shift", like our recent report of a core rearrangement of a dimer-of-dimers to an adamantane core,[43] is a possible explanation for changes in the metal−metal distance observed for advancement from S_2 to S_3 and S_3 to S_0. We are currently exploring further conditions that promote a core shape-shift from a dimer-of-dimers to an adamantane core, as well as conditions that might promote the rearrangement of an adamantane to a dimer-of-dimers for Mn−oxo adamantanes, such as those reported here.

Although the exact coordination environment is a matter of ongoing investigation, it is generally believed that the Mn−oxo complex of the OEC is coordinated predominantly by carboxylates from aspartate and glutamate, along with oxide bridges and one or two imidazoles.[8,9,15,16] Substitution reactions of **1** with iminodicarboxylates afforded complexes **8**−**11** that more closely approximate the coordination environment of PSII and that very likely could not have been

(133) The highest pK_a among the $[Mn_4O_6]^{4+}$ adamantane cores of 12.5 in acetonitrile for the first protonation of $[Mn_4O_6(tame)_4](CF_3SO_3)_4$, was determined by spectrophotometric titration with pyridinium triflate in acetonitrile. A corresponding aqueous pK_a of 5.0 is estimated using the relation pK_a(H_2O) = pK_a(CH_3CN) − 7.5 (Kristjansdottir, S. S.; Norton, J. R. In *Transition Metal Hydrides*; Dedieu, A., Ed.; VCH Publishers: New York, 1992; pp 309−359) (Dubé, C. E.; Armstrong, W. H. unpublished results).

(134) Baldwin, M. J.; Stemmler, T. L.; Riggs-Gelasco, P. J.; Kirk, M. L.; Penner-Hahn, J. E.; Pecoraro, V. L. *J. Am. Chem. Soc.* **1994**, *116*, 11349−11356.

(135) Kristjansdottir, S. S.; Norton, J. R. Transition Metal Hydrides. In *Transition Metal Hydrides*; Dedieu, A., Ed.; VCH Publishers: New York, 1992; pp 309−359.

(136) We also noted a trace level of another species, whose resonances are similar to those of **1**H^+ and which we believe derives from protonation of oxo ligand(s) lying in the plane perpendicular to the C_2 axis.

(137) Wieghardt, K. *Angew. Chem., Int. Ed. Engl.* **1989**, *28*, 1153−1172.

prepared under the oxidation conditions utilized in self-assembly of high-valent manganese−oxo complexes. Furthermore, the unique substitution chemistry of **1** with R-ida ligands afforded asymmetrically ligated complexes, the mixed ligand nature of which is most likely unachievable using self-assembly synthetic methods.

A special feature of the asymmetrically ligated complexes **8**−**11** is the substantial site differentiation of the oxo bridges of the $[Mn_4O_6]^{4+}$ cores as revealed by protonation. In a number of metalloenzymes, site-specific tuning of the chemical reactivity of the active site is achieved through a combination of coordination of amino acid residues, steric interactions between the metal ions and amino acid residues, and hydrogen bonding. Such factors are difficult to incorporate, however, into structural models of metalloenzymes synthesized by spontaneous self-assembly. Some Mn−oxo dimeric systems have achieved oxo bridge discrimination by the asymmetric coordination of different ligands to the metal ions, as demonstrated in the solid-state structure of [(Me_3-tacn)Mn(μ-O)$_2$(μ-OAc)Mn(η^2-OAc)(η^1-OAc)] and [(Me_3-tacn)Mn(μ-O)$_2$(μ-OAc)Mn(bpy)(MeOH)](ClO_4)$_2$ complexes.[138] In contrast to the subtle oxo bridge site differentiation in **1**, asymmetric ligation of **11** has substantially altered the oxo bridge electron density to afford essentially a single protonation isomer. The differentiated sites within complexes **8**−**11** using iminodicarboxylate ligation demonstrates how amino acid side chains might similarly differentiate the site of substrate binding within the Mn complex of the OEC.

One of the current proposals for water oxidation suggests that a Mn^V═O species[57−61] may be a key reactive intermediate in the O−O bond-forming step. In this regard, the electrochemistry of the carboxylate complex **11** is of particular interest, since it has the lowest (V, IV, IV, IV)/(IV, IV, IV, IV) redox couple of the known adamantane-shaped $[Mn_4O_6]^{4+}$ complexes and, as such, is an attractive candidate for isolation and reaction studies of stable Mn^V−oxo model compounds.

Acknowledgment. We thank Prof. D. W. Wright for helpful discussions of the interpretation of ^{1}H NMR spectra. Funding for this research was provided by the National Institutes of Health grant GM38275. The National Institutes of Health grant 1 S10RR09008 and Boston College provided funds for purchase of a Siemens SMART single crystal X-ray diffractometer. The W.M. Keck Foundation provided funds for the SQUID magnetometer at Tufts University. The Micromass Quattro mass spectrometer at the University of Illinois Mass Spectrometry Laboratory was purchased in part with a grant from the Division of Research Resources, National Institutes of Health (RR 07141).

Supporting Information Available: A description of the synthesis of *N*-cyclopentyliminodiacetic acid, *N*-*tert*-butyliminodiacetic acid, and (Bu_4N)$_2$(me-ida); a table of yield, elemental analysis and ^{1}H NMR data for (*n*-Bu_4N)$_2$(R-ida) and (*n*-Et_4N)$_2$(R-ida); a description of the synthesis of *cis*,*cis*-1,3,5-triaminocyclohexane; a description of the synthesis of **9** and **10**; tables of yield, elemental analysis, ESI-MS, UV−vis, electrochemistry, IR, and ^{1}H NMR data for **4**−**11**; ESI mass spectra of **4**−**6**, **9**−**11**; $\chi_M T$ versus T plots for **4** and **8**, a M (μ_B/mol) versus $\mu_B H/kT$ plot for **1**; ^{1}H NMR spectra of **4**, **5**, **6**, and **9**; plots of nonlinear least-squares fit of absorbance versus pH for titration of **8** and **11**; and full crystallographic information for **7** and **11**, including figures illustrating hydrogen bonding. This material is available free of charge via the Internet at http://pubs.acs.org.

IC050183W

(138) Bossek, U.; Saher, M.; Weyhermuller, T.; Wieghardt, K. *J. Chem. Soc., Chem. Commun.* **1992**, 1780−1782.